Sulfur Defect Engineered Biodegradable Cobalt Sulfide Quantum Dots Driven Photothermal and Chemodynamic Anti-Cancer Therapy

By Houjuan Zhu

WORD COUNT 10273 TIME SUBMITTED 27-MAY-2022 11:42AM
PAPER ID 86556959

Sulfur Defect Engineered Biodegradable Cobalt Sulfide Quantum Dots Driven Photothermal and Chemodynamic Anti-Cancer Therapy

Houjuan Zhu,[a, c, f, ‡, *] *Shuyi Huang,*[a, b, ‡] *Mengbin Ding,*[d] *Zibiao Li,*[c] *Jingchao Li,*[d,*] *Suhua Wang,*[a, e,*] *David Tai Leong*[a,*]

[a]Department of Chemical and Biomolecular Engineering, National University of Singapore, 4 Engineering Drive 4, Singapore 117585, Singapore

[b] College of Environmental Science and Engineering, North China Electric Power University, Beijing 102206, P. R. China

[c]Institute of Materials Research and Engineering, A*Star (Agency for Science, Technology and Research), Singapore, Singapore

[d]Shanghai Engineering Research Center of Nano-Biomaterials and Regenerative Medicine, College of Chemistry, Chemical Engineering and Biotechnology, Donghua University, Shanghai 201620, P.R. China

[e]Guangdong Provincial Key Laboratory of Petrochemical Pollution Process and Control, School of Environmental Science and Engineering, Guangdong University of Petrochemical Technology, Maoming, Guangdong 525000, P. R. China.

[f]Centre for Advanced 2D Materials, Graphene Research Centre, National University of Singapore, Singapore 117546, Singapore.

*Corresponding author. E-mail: cheltwd@nus.edu.sg; zhu_houjuan@imre.a-star.edu.sg; wangsh@gdupt.edu.cn;-jcli@dhu.edu.cn.

‡ Equal contributions

KEYWORDS: Sulfur defect, Cobalt sulfide quantum dots, Photothermal therapy, Chemodynamic therapy, Anti-cancer therapy, Fenton-like reaction

ABSTRACT: Chemodynamic therapy (CDT), as a powerful tumor therapeutic approach with low side effect and selective therapeutic efficiency, has gained much attention. However, low intracellular content of H_2O_2 and the cellular bottleneck of low intracellular oxidative reaction rates at tumor sites limited the anti-tumor efficacy of CDT. Herein, a series of sulfur-deficient engineered biodegradable cobalt sulfide quantum dots (CoS_x QDs) were constructed for improved synergistic photothermal and hyperthermal enhanced chemodynamic therapy of tumor through regulating photothermal conversion efficiency (PCE) and Fenton-like activity. Through defect engineering, we modulated PCE and promoted the Fenton

catalytic capability of CoS_x QDs. With defect sites increasing, Fenton-like activity was improved to generate more toxic •OH while photothermal effect slightly declined. In light of above unique superiorities, the best synergistic effect of CoS_x QDs were obtained through comparing their PCE and catalytic activity by regulating the sulfur defect fractions degree in these QDs during synthetic process. In addition, ultra-small size and biogradation endowed QDs with the ability to be rapidly decomposed to ions that was easily excreted after therapy, thus reducing biogenic accumulation in the body with lowered the systemic side effects. I*n vitro/vivo* results demonstrated that the photothermal and hyperthermal enhanced chemodynamic effect of CoS_x QDs can enable remarkable anticancer properties with favorable biocompatibility. In this study, the defect-driven mechanism for photothermal enhanced Fenton-like reaction provides a flexible strategy to deal with different treatment environments, holding great promise in developing multifunctional platform for cancer treatment in the future.

INTRODUCTION

Cancer remains to be one of the most devastating illnesses with a high fatality rate. Over the past decade, considerable effort has been made on cancer therapy treatments including immunotherapy, photothermal therapy (PTT), photodynamic therapy (PDT).[1-7] Lately, chemodynamic therapy (CDT) has gained increasing level of interest due to its spontaneous and endogenous chemical driven cytotoxicity without the need of extrinsic interference.[8, 9] It utilizes metal-based Fenton agents to split intracellular hydrogen peroxide (H_2O_2) into more reactive hydroxyl radicals (•OH), which then tip the balance of redox/oxidation states within the cancer cells and drive organellar damages within the cells.[10-12] The cancer cells' unique tumor microenvironment (TME) conditions of high local H_2O_2 concentration and an acidic pH only primes the tumor site for the pro-death oxidative Fenton reaction whilst sparing normal and healthy tissues where the TME conditions are absent.[13, 14] It may sound promising, however the optimal pH condition for a robust Fenton reaction for cancer therapy purposes resides in the extremes of cellular pH of less than pH 4 which unfortunately is not inherent in the TME. This limitation thus greatly

narrows the scope of use of any conventional Fenton reaction driven CDT. Such point drives us to improve the reaction rate of a metal-based Fenton reaction even in a less acidic (and unfavorable) condition.

Arrhenius' equation correlates that the rate of reaction in general doubles with a 10 ^{o}C increase in reaction temperature[15-17] At face value, this sounds promising but there is a limit that how high we can elevate a given patient's core temperature. But we can raise the local temperature of the tumor with high precision and in a localized area. Therefore, we aim to directly increase the reaction rate of CDT at the tumor site with synergistic photothermal means. Due to the small but concentrated local heating of the tumor, we in essence can simultaneously spare the normal healthy tissues.[18-21] In order to ensure the increased temperature is to be localized at the CDT site without any room of error, we sought to design a nanoplatform that has duality in increasing localized heat generation through rolling photothermal activation and dissipation and a Fenton agent into one single entity. Photothermal therapy (PTT), which utilizes photothermal nanoagents to convert external near-infrared (NIR) light into heat, could not only collaborate with CDT for thermal accelerated-Fenton reaction by increasing local temperature of tumor, but also further boost the cytotoxicity through thermal ablation of the same spot at the tumor. Despite the synergistic PTT and CDT nanoagents have extensively been reported,[9, 22-24] all these combinations are a mixture of two or more nanomaterials in a functionally additive approach and not as a single inseparable platform. These earlier approaches are prone to dislodge various nanocomponents or functionalization within the body and can result in segregated efficiencies, such as photothermal heating in a location where there are no Fenton agents or vice versa. The segregation would then defeat the entire intent of having a dual PTT-CDT system in the first place.

Transition metal dichalcogenides (TMDs) quantum dots (QDs), such a cobalt sulfide (CoS_x), have attracted some attention because of several advantages including atomic-scale thickness, direct bandgap and favorable electronic properties.[25] The intrinsic existence of multivalency in Co coupled with a wide

absorption range in a NIR window might present CoS_x species as a potential candidate for our PTT/Fenton related CDT therapeutic agents.[26-28] We have earlier defect engineered at least 7 other TMDs based on a biomineralization assisted bottom-up strategy, in which some natural biopolymers like BSA were used as surfactant to render nanoparticle with uniform size and excellent biocompatibility due to their template effect.[20, 29-31] By controlling stoichiometric molar ratios at the synthesis stage, tunable sulfur vacancy density and oxygen and hydroxyl defects with more variable electronic trap states could be engineered into the TMDs QDs. Herein, we defect engineered defects to further regulate the CDT and PTT effect of CoS_x QDs.[5, 29, 32]

Herein, for the first time, we designed a facile and mild strategy to synthesize a series of biocompatible cobalt sulfide quantum dots of variable degree of defects (collectively designated as CoS_x QDs), which enable accurately control of photothermal conversion efficiency (PCE) and Fenton-like activity by defect engineering. These defect-engineered CoS_x QDs exhibit tunable optical and electrical properties to optimize synergistic therapeutic effect of PTT and CDT (Scheme 1). These various defect engineered CoS_x QDs group can induce cancer cell death in four simultaneous processes: (1) Fenton-like reaction, CoS_x QDs catalyze endogenous hydrogen peroxide (H_2O_2) to product more harmful ROS, which could lead to the oxidative damage to cancer cell; (2) perturbing the cellular antioxidant defense system through a redox reaction that transfers GSH into GSSG for enhancing ROS generation; (3) ablating cancer cells by the photothermal effect of CoS_x QDs; (4) heat generated by photothermal conversion process enhanced the Fenton reaction rate between CoS_x QDs and endogenous H_2O_2. Additionally, the degradability and hypotoxicity of CoS_x QDs may lead to efficient metabolization and clearance, promising favorable biocompatibility and biosafety. Therefore, defect-driven CoS_x QDs can serve as a tumor-specific multifunctional agent with flexible and controllable efficacy for the cancer therapy in the future.

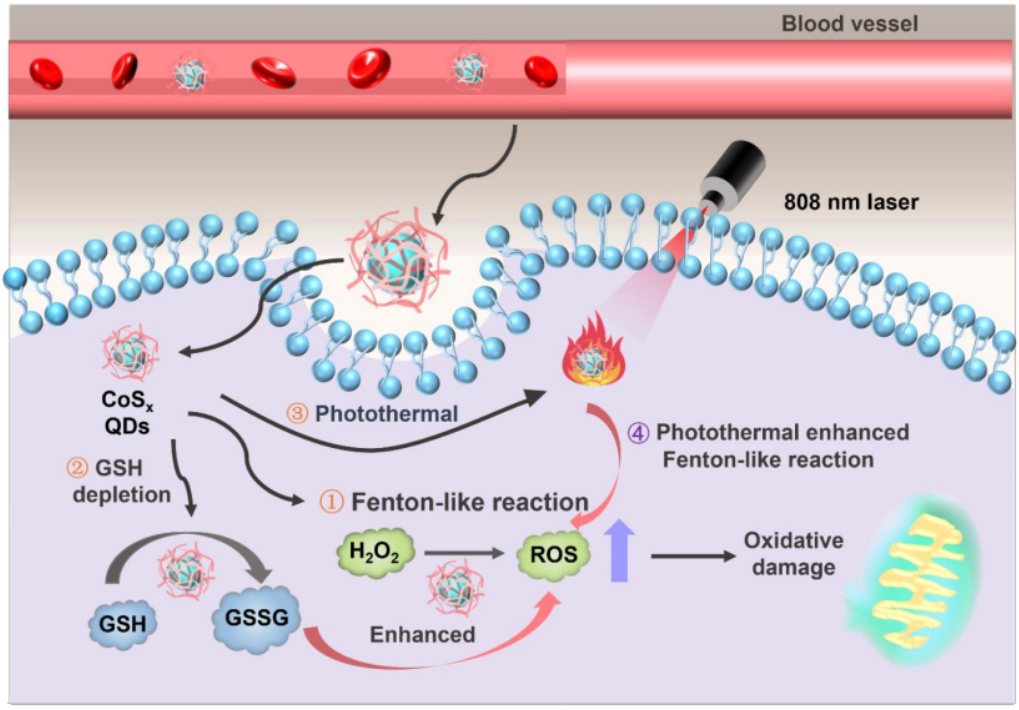

Scheme 1. Schematic illustration of biodegradable CoS_x QDs for photothermal therapy and hyperthermal-enhanced chemodynamic therapy of tumor.

RESULTS AND DISCUSSION

Characterizations of CoS_x QDs. The defect-engineered CoS_x QDs were prepared and characterized *via* a biomineralization assisted bottom-up method, as shown in **Figure 1A**. The solution-processed CoS_x QDs were obtained within a few seconds through adjusting pH values. During this process, bovine serum albumin (BSA) was applied as surfactant and stabilizer to control size. To study defect engineering, CoS_x QDs with different sulfur defects were prepared through varying the initial feed molar ratios of Co^{2+} and S^{2-} (1:0.5, 1:1, 1:2, 1:4, 1:6 and 1:8 and termed as CoS_x QDs 1:0.5, CoS_x QDs 1:1, CoS_x QDs 1:2, CoS_x QDs 1:4, CoS_x QDs 1:6 and CoS_x QDs 1:8). Transmission electron microscopy (TEM) estimated the primary size of ultra-small CoS_x QDs 1:2 to be around 5.8 nm, showing a uniform size distribution and no observable aggregation of QDs (**Figure 1B**). Additionally, to investigate the effect of initial molar ratios on size, the hydrodynamic size of CoS_x QDs with different sulfur amounts ranged from 7.0 ~ 40 nm (**Figure S1A**). Simultaneously, CoS_x QDs with different molar ratios of Co to S exhibited superior stability in different solution even stored for 25 days probably due to more BSA coating, implying its suitability for biological applications (**Figure S1B**). UV-vis spectra of CoS_x QDs displayed an ultrawide absorption band from visible to NIR range and the increased NIR absorbance with decreasing molar ratios of Co/S (the amount of S increasing), offering great potentials in photothermal field (**Figure 1C**). The increased absorbance may be due to improved electron density in QDs structure, resulting from defect sites generation. Correspondingly, to investigate such point, the less intensive tail absorbance in the less sulfur samples reflected the wider optical bandgap (**Figure 1D**, **Figure S2**). In summary, the physical and chemical properties of CoS_x QDs could be easily regulated by adjusting sulfur level in samples, giving the opportunity to tune properties for more effective synergism between the photothermal and chemodynamic properties. The crystalline structures of CoS_x QDs with different sulfur contents were assessed by X-ray diffraction (XRD) (**Figure 1E**). Comparing the XRD of CoS_x QDs 1:0.5 or 1:1 with bare BSA (**Figure S1C**), the broader diffraction peaks (2θ) at 30.5° found in the latter were consistent with the standard data of Co_9S_8 (JCPDS No. 65-6801). With sulfur amount further increasing, distinct

peaks at 34.5° could be also observed and identical with the values reported in the literature for $Co_{1-x}S$ (No. 42-0826), suggesting the multi-component crystalline mixtures. The broad reflection peaks width was in accordance with the XRD features of zero-dimensional nanomaterials, indicating the small sizes of the samples.[29] More importantly, the crystal phase transition commonly corresponded to the grain coordination number in spatial scale, reflecting a probable variation of valence for both cobalt and sulfur atoms, which was considered to be closely tied to the amount of sulfur vacancy in CoS_x QDs.[33, 34] Then, X-ray photoelectron spectroscopy (XPS) was further employed to assess surface valance states of cobalt and sulfur element in CoS_x QDs with different sulfur levels. From the curve-fitting of Co 2p3/2 peak (**Figure 1F**), the peaks of 779 and 781.1 eV were related to Co^{3+} and Co^{2+}, respectively. XPS quantification of the valence states revealed that Co(III) gradually replaced Co(II) as the major chemical status of Co element, suggesting partial oxidation of cobalt ions as the ratio of Co/S decreased, which arisen from the low redox potential of Co^{3+}/ Co^{2+} (≈0.45 V). Similar oxidation phenomenon was also found from the high resolution XPS spectra of S 2p region. As depicted in **Figure 1G**, the S^{2-} 2p3/2, S_2^{2-} 2p3/2, S_x^{2-} 2p3/2 and SO_n^{x-} peaks can be observed at 161.4, 162.1, 163.6 and 168.0 eV, respectively. Except for the S_x^{2-} 2p3/2 peak assigned to the sulfur of BSA, the proportion of S_2^{2-} increased as the molar ratio of Co/S decreased, providing a direct evidence for the reduce of sulfur vacancies with the sulfur amount increasing in synthesis process. Meanwhile, this change in sulfur vacancies generally presumed a decreasing defect level and thus improves on the crystallinity, which was in accordance with the XRD spectra.

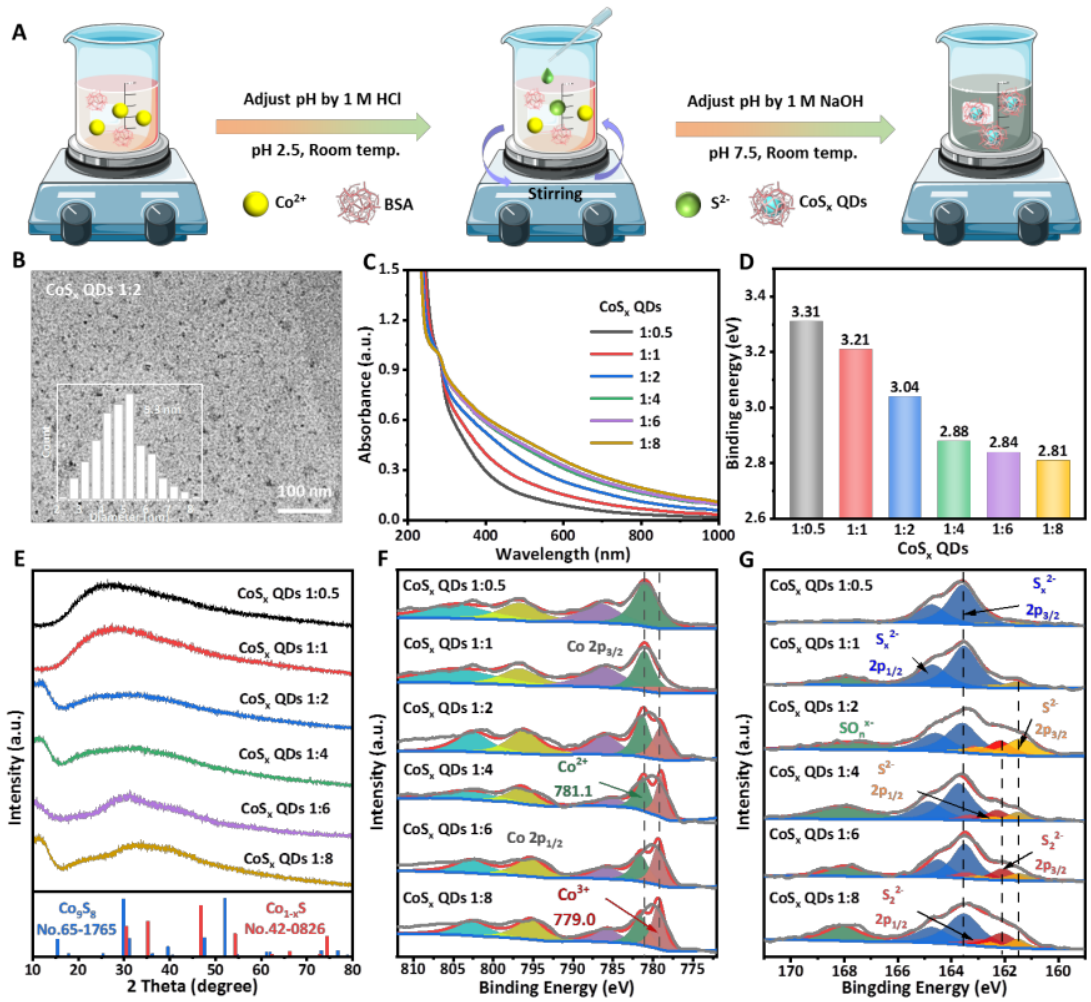

Figure 1. Characterization of CoS_x QDs. (**A**) Illustration for synthesizing differently sulfur contained CoS_x QDs; (**B**) TEM image and size distribution of CoS_x QDs 1:2; (**C**) UV spectra and (**D**) bandgap energy of differently sulfur contained CoS_x QDs; (**E**) XRD pattern; High resolution XPS spectra of the (**F**) Co 2p region and (**G**) S 2p spectra of CoS_x QDs.

Photothermal performance of CoS_x QDs. Inspired by the strong absorbance in NIR region, the photothermal property of CoS_x QDs with different sulfur vacancy level was investigated in PBS 6.5 solution under NIR laser irradiation (808 nm, 0.8 W/cm^2) (**Figure 2A**). The molar absorbance coefficients of CoS_x QDs were firstly calculated using CoS_x QDs dispersions at different concentrations (**Figure 2B**). These plots between the absorbance at 808 nm and concentrations of CoS_x QDs were found to be linear,

and the molar extinction coefficient of defect-engineered CoS_x QDs at 808 nm increased with its rising sulfur level and attained a maximum of 7.44×10^3 $M^{-1} cm^{-1}$ when the molar ratios of Co/S reached 1:8. Such changing trend could also be observed from the photothermal conversion efficiencies (PCE) of CoS_x QDs with different defect levels, which were calculated following by the Roper's method from the fitting of cooling curve after tuning the concentration of all CoS_x QDs groups to reach the same absorbance at 808 nm (**Figure 2C**). As presented in **Figure 2D**, sulfur-rich CoS_x QDs exhibited better photothermal performance and the PCE of CoS_x QDs 1:8 even attained 40.5 %, which was higher than that of the most reported inorganic photothermal agents (**Figure 2E**).[35-38] Additionally, the infrared thermal images of different concentrations of CoS_x QDs 1:2 was further monitored to directly demonstrate the excellent photothermal conversion capability of CoS_x QDs, where a high imaging intensity contrast corresponding to solution temperature was observed to increase with the increase in the CoS_x QDs concentration and the irradiation duration (**Figure 2F**). The solution temperature risen in 5 min and gave sensitive response to the concentration of CoS_x QDs, suggesting a concentration-dependent photothermal heating effect. More extensive data was collected on complete heating-cooling procedure and presented in **Figure 2G**. The solution temperature could be raised from 21 °C to 55 °C after 5-min laser irradiation even at a low CoS_x QDs 1:2 concentration of 1.0 mM, which was higher than the critical temperature (42 °C) for the induction of cancer cell apoptosis, while water exhibited negligible temperature increase (less than 3 °C). Besides of the excellent PCEs of CoS_x QDs, photothermal stability is also a prerequisite for photothermal agents. The temperature changes of all CoS_x QDs (1.0 mM) dispersions were monitored for different irradiation cycles. The maximum temperatures of CoS_x QDs still maintained the same high level even after a repeating heating-cooling operation for 5 cycles, while a commercial NIR photothermal agent indocyanine green (ICG) for clinical application approved by US Food and Drug Administration greatly degraded upon five repeated irradiation cycles (**Figure 2H**).[39] The excellent photothermal property and stability of CoS_x QDs proved their potential for photothermal cancer therapy applications.

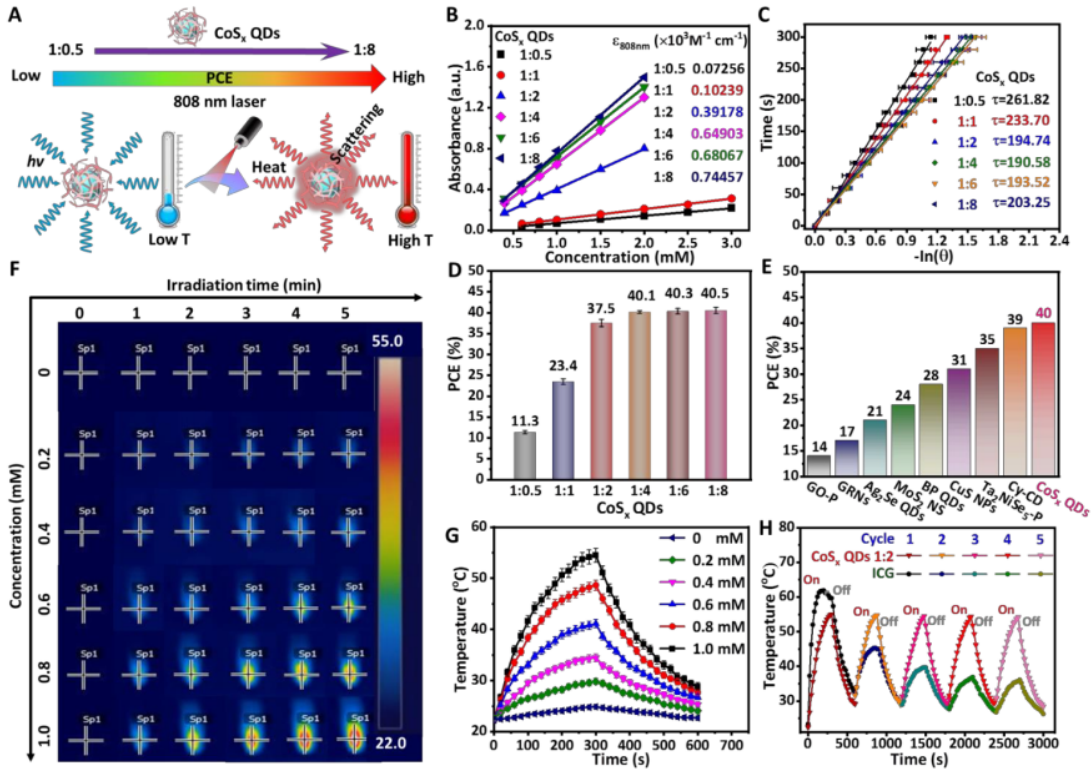

Figure 2 Influence of sulfur vacancies on photothermal performance of CoS_x QDs. (**A**) The photothermal mechanism and the defect-engineered control of CoS_x QDs in photothermal conversion efficiency (PCE); (**B**) The calculation of molar absorptivity at absorbance of 808 nm laser (0.8 W/cm^2); (**C**) Time constant for heat transfer of CoS_x QDs by applying the natural logarithm of temperature change versus time data; (**D**) PCEs of differently sulfur contained CoS_x QDs; (**E**) The comparison of photothermal conversion efficiency with other typical quantum dots photothermal nanomaterials reported in the literature; (**F**) Infrared thermal images of CoS_x QDs 1:2 at different concentration under the exposure of 808 nm laser (power density: 0.8 W/cm^2) for 5min and (**G**) corresponding photothermal heating curves; (**H**) Photothermal stability of CoS_x QDs 1:2 (1.0 mM) and ICG under the photothermal heating and nature cooling cycles by the 808-nm laser irradiation.

Fenton-like properties of CoS_x QDs. The Fenton-like reaction and H_2O_2 consumption mediated by the defect-engineered CoS_x QDs were firstly evaluated in a cell-free system by employing 3,3'-diaminobenzidine tetrahydrochloride (DAB) as chromogenic agents to indicate •OH-generation (**Figure 3A**). And the reaction process of different sulfur level CoS_x QDs was recorded by UV absorption spectrum (**Figure S3**). After CoS_x QDs 1:2 was added into reaction system (DAB and H_2O_2), a new

absorption band at 569 nm was enhanced as reaction time prolonged (**Figure 3 A1**), accompanying by an obvious visual color change from light brown to black within 20 min (the insert picture), indicating the occurrence of Fenton-like reaction. Then, kinetics analysis of different sulfur level CoS_x QDs was taken out to give more comprehensive assessment on catalytic efficiency and •OH-generating abilities at various reaction points (**Figure S4**). By the standardized analysis of kinetics analysis, the reaction rates of defect-engineered CoS_x QDs (kinetic ratio of CoS_x QDs + DAB + H_2O_2 and CoS_x QDs +DAB) were obtained and shown in **Figure 3 A2**. It was observed that the samples with higher sulfur content displayed a better catalytic activity at the first few seconds, then the catalytic rate slowed down and finally exhibited lower catalytic degree on a timescale of minutes, revealing that the catalytic rate was strongly related to reaction time and sulfur level in catalysts. Given that the CDT treatment was a relatively extended period, the amounts of generated radicals at 20 min were standardized for a comparative study, as shown in **Figure 3 A3**. Compared with their corresponding control groups (CoS_x QDs + probe or H_2O_2 + probe), the absorbance of CoS_x QDs/probe/ H_2O_2 group decreased with the increased sulfur contents in the QDs, showing that the amount of radicals generated by CoS_x QDs 1:0.5 was less than that by CoS_x QDs 1:1. Additionally, another chromogenic agent 3,3',5,5'-tetramethylbenzidine (TMB) was also employed to monitor the process of Fenton-like reaction (**Figure S5 A**). It was clearly observed that a new peak was gradually formed at ~ 665 nm within 20 min and the colorless TMB was oxidized to blue oxTMB. According to the reaction kinetics at 665 nm (**Figure S5 B**), the catalytic rates of defect-engineered CoS_x QDs were showed to be related to the sulfur amounts in QDs, which was in accordance with that of DAB. Simultaneously, only QDs 1:0.5, 1:1, 1:2 groups showed the dramatic increase in absorbance after 20 min of reaction, suggesting a better CDT performance over the other three CoS_x QDs types (**Figure S5 C**). Moreover, MB degradation was also investigated to confirm the catalytic activity of Fenton-like reaction (**Figure 3B**). As shown in **Figure 3 B1**, MB could be quickly degraded around 30 min when CoS_x QDs 1:2 were added into H_2O_2/MB system. Under the same condition, H_2O_2 without CoS_x QDs was observed to have no capability to degrade MB, indicating that the degradation of MB was indeed induced by

radicals from the reaction between CoS_x QDs and H_2O_2 (**Figure S6**). The better catalytic performance of QDs 1:0.5, 1:1, 1:2 and 1:4 groups achieved 80 % degradation rate of MB within 20 min, but their reaction efficiencies in the first 10 min varied from one other (**Figure 3 B2**). Then, a pseudo-first-order kinetics rate constant in the first 10 min were obtained by linear fitting (**Figure 3 B3**). As expected, CoS_x QDs 1:1 showed the best degradation performance among all six CoS_x QDs groups with the kinetic rate constant around 0.075 (min^{-1}) and their rate constants significantly decreased with S/Co ratios increasing, which was in accordance with the previous result using probe DAB and TMB. Summarizing these data, it became evident that the defect chemistry in the as-developed CoS_x QDs promoted the efficiency of Fenton-like reaction. We also have evaluated the influence of glutathione (GSH) on •OH-induced MB degradation and the GSH depletion process by CoS_x QDs (**Figure 3C**). Nearly all the MB was degraded without the presence of GSH. The degradation process was greatly inhibited by the increasing GSH concentration. Even at a low MB concentration of 1.0 mM, the degradation efficiency of MB reduced to 55 %, confirming the ROS-elimination property of GSH (**Figure 3 C1**). Then the GSH depletion-enhanced chemodynamic efficacy was further investigated through introducing exogenous •OH-generating catalyst Cu^{2+}, which have been widely revealed as a Fenton-like reagent to generate radicals from H_2O_2 (**Figure 3 C2**). MB was thoroughly degraded by Cu^{2+} and H_2O_2, however the degradation process could be completely restrained with the presence of GSH. And most particularly, this delicate balance between GSH depletion and Fenton-like reaction was broken when CoS_x QDs 1:2 was added to the reaction system, which led to more than 60 % degradation of MB after 3 h of reaction. The above phenomenon suggested that CoS_x QDs indeed took an important role in GSH-depletion process. Moreover, additional control groups were taken for a more detail comparison to exclude the effect of catalyst Cu^{2+} (**Figure 3 C3**). After reaction with only Cu^{2+} for 3 hours, 0.1 mM CoS_x QDs 1:2 were added into reaction system. Remarkably, the addition of 0.1 mM CoS_x QDs 1:2 remarkably enhanced MB degradation in the next 20 min, even showing a higher degradation rate than that of Cu^{2+}-CoS_x QDs group. Such phenomenon proved the cascade catalytic activity of CoS_x QDs, which could deplete GSH by the

chemical valence transition between Co^{3+} and Co^{2+} through this redox reaction: $2Co^{3+} - CoSx\ QDs + 2GSH \rightarrow 3Co^{2+} - CoSx\ QDs + 2GSSG$.[40] Such good performances revealed the intensified chemodynamic activity of CoS_x QDs, offering them good potential in CDT against cancer cells.

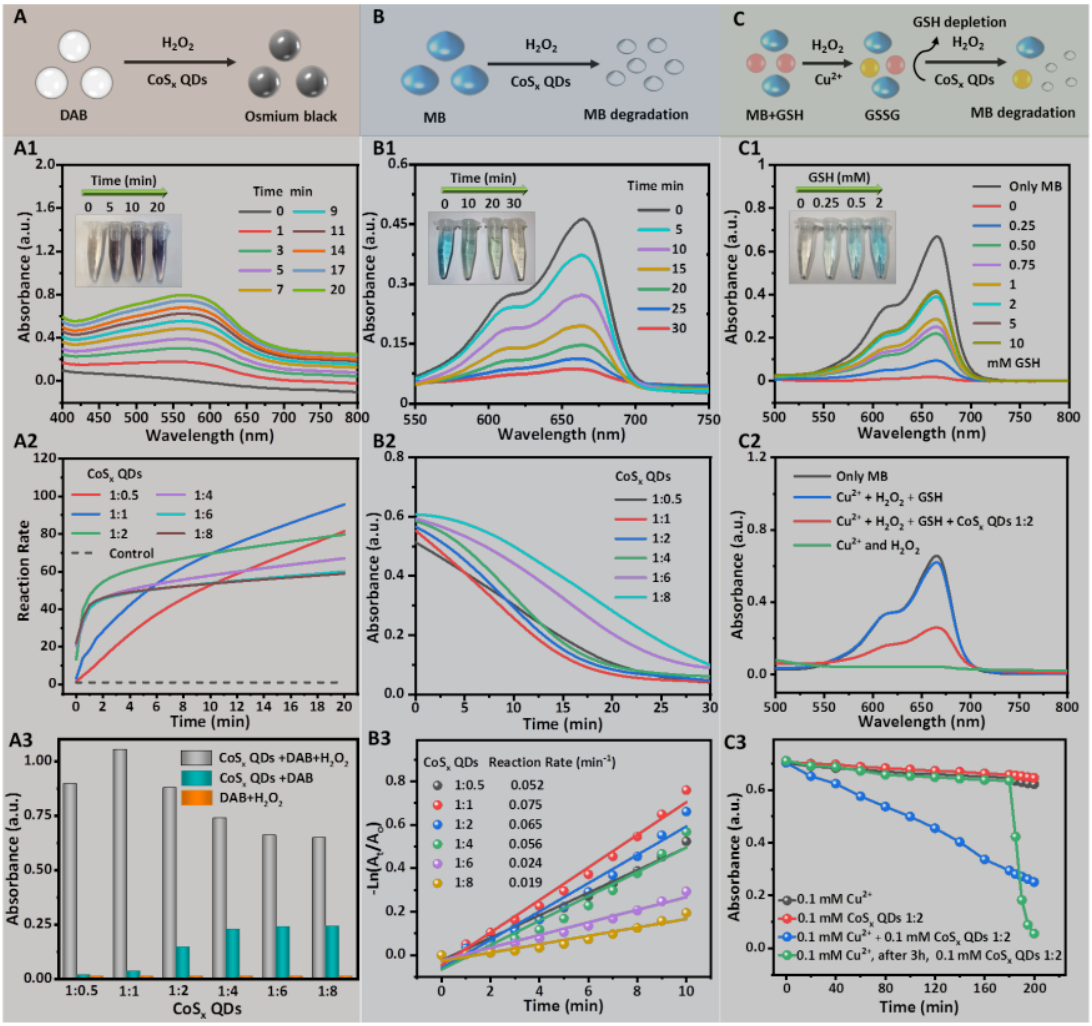

Figure 3. The influence of defect engineering on the catalytic rate of Fenton-like reaction and the GSH depletion by CoS_x QDs. (**A**) The evaluation of OH• production using probe DAB at pH = 6.5 (**A1-A3**, UV spectra of reaction systems at different time, the kinetics of catalytic reactions and the UV absorbance of different reaction systems at 20 min, respectively); (**B**) MB degradation by Fenton-like reaction of CoS_x QDs in $NaHCO_3$ solution. (**B1-B3**), MB degradation by CoS_x QDs 1:2, MB degradation kinetics in different reaction systems, and corresponding reaction rate obtained by first order kinetic model, respectively); (**C**) GSH protection on MB degradation by CoS_x QDs 1:2, (**C1**) impact of different

GSH concentrations on MB degradation by CoS_x QDs 1:2, the GSH depletion by CoS_x QDs 1:2, (**C2**) degradation degree after 3 h and (**C3**) degradation kinetics with different catalyst components in MB/H_2O_2 solution, $C(Cu^{2+})$ = 0.1 mM, C(CoS_x QDs) = 0.1 mM, C(GSH) = 1.0 mM, $C(H_2O_2)$ =50 mM.

Hyperthermal-enhanced chemodynamic therapy *in vitro* and the biodegradation of CoS_x QDs. According to the above-mentioned results, both photothermal and chemodynamic properties of CoS_x QDs displayed a remarkable sulfur amount dependence. In particular, the sulfur-deficient design of CoS_x QDs enhanced the Fenton-like reaction but reduced its PCE. Despite that, CoS_x QDs 1:2 samples showed a relatively high PCE and MB degradation rate simultaneously. So that the synergistic effect of CDT and PTT might lead to a higher therapy efficiency of CoS_x QDs 1:2 than that of other sulfur level groups, thus CoS_x QDs 1:2 samples were chosen in the following experiments. Based on this, the photothermal-enhanced Fenton-like reaction was investigated using DAB as the ROS indicator under three temperature regimes (**Figure 4A** and **4B**). It was found that the higher temperature used in the experiment, the faster catalytic rate was observed. Notably, after 5 min reaction, 50 °C-group exhibited the highest catalytic efficiency, which was respectively about 1.2 times and 2.5 times higher than that when at 40 °C and at 20 °C. The electron spin resonance spectrum (ESR) was employed to give a more reliable result (**Figure 4C**). A stronger ESR signal was observed from the high temperature group (pH = 6.5, 40 °C), demonstrating that the heat could enhance the ROS generation and accelerate CDT effect. Meanwhile, under the same temperature, the •OH signal at pH = 6.5 was higher than that at pH = 7.4, suggesting that more •OH were generated in acidic conditions, thus further showing their high therapy efficacy of tumor with lowered side effect against normal tissue.

Although various inorganic nanoparticles have been proved to exhibit outstanding performance in the field of nanomedicine, it is remarkably hard for their clinical translation due to the long-term distribution *in vivo* and potential toxicity that gave rise to the ROS generation when exposed to cellular environments.[41] Owing to the higher basal level of oxidative stress in cancer cells, the controlling of nanoparticle concentration *in vivo* is essential in generating a moderate level of ROS that would just exceed toxic thresholds in cancer cells but not normal cells.[42] Apart from that, the biodegradation of

nanoparticles also gained necessary attention that could protect the normal cells from irreversible and unnecessary damage. Based on this, degradation experiments of CoS_x QDs were further designed under different pH value and temperature (**Figure 4D** and **4E**). It was clear that the color of CoS_x QDs 1:2 solution slowly changed from dark brown to tawny and then to nearly colorless, indicating the release of cobalt ions into aqueous solution arising from the self-degradation of CoS_x QDs. The degradation rate in mildly acidic condition (pH = ~6.5, extracellular environment in cancer tissue) was higher than that in neutral conditions (pH = ~7.4, normal tissues), suggesting that the QDs could be quickly degraded at tumor sites after therapy, thus reducing *in vivo* accumulation with less systemic side effects. While in normal tissues, ROS generation is limited by neutral conditions and low level of H_2O_2 that protect normal tissues from being destroyed. Meanwhile, the rising of temperature could also accelerate this degradation process, indicating the PTT could enhance CDT effect through a rising temperature.

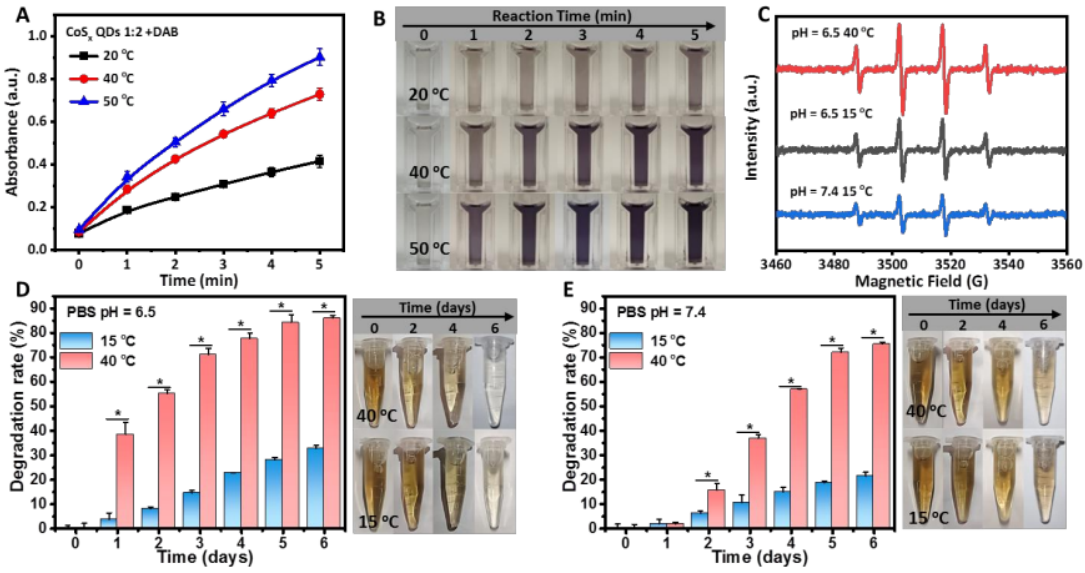

Figure 4. Thermal enhanced ROS generation and accelerated degradation of CoS_x QDs. (**A**) Fenton-like reaction of CoS_x QDs 1:2 under different temperature using DAB as the ROS probe and (**B**) corresponding photograph of the reaction in different time points; (**C**) ESR spin trap signals of DMPO-•OH under different conditions; degradation of CoS_x QDs at (**D**) pH = 6.5 and (**E**) pH = 7.4 (The right figure is the degradation pictures of CoS_x QDs). Degradation rate = $(A_0-A)/A_0$; A and A_0 is the

absorbance of QDs at the given Day and Day 0, respectively. The data are presented as the mean ± s.d., n = 5. The statistical significance was calculated via Student's t-test, *P < 0.05.

Defect-driven mechanism for regulating photothermal effect and Fenton-like activity. The reaction mechanism of defect engineered CoS_x QDs for tunable photothermal enhanced CDT were further confirmed by investigating the effect of a change in cobalt valence state, as depicted in **Figure 5 A** and **5B**. As the initial molar ratios went up from 1:0.5 to 1:8, the trivalent cobalt (Co^{3+}) level appeared and increased to 47.2 %, accompanied by a significant enhancement of both PCE and molar absorption coefficient at 808 nm. This may be attributed that the increased Co^{3+} in QDs could narrow the band energy, thus inducing the widen absorption, lastly enhancing the PCEs. Simultaneously, the Fenton-like activity in 20 min reduced with the amount of bivalent cobalt (Co^{2+}) decreasing. Thus, it appeared that cobalt valence played a crucial role in synergistic PTT/CDT. Besides, from the kinetics using DAB as chromogenic agent, it was found that the rate and extent of Fenton-like reaction were correlated to the molar ratio of Co/S. Thus, ESR technology was further employed to monitor dynamics of Fenton-like reaction, using 5,5-dimethyl-1-pyrroline-N-oxide (DMPO) and 2,2,6,6-tetramethylpiperidine (TEMP) as spin-trapping reagents for the capture of •OH or O_2^-. As shown in **Figure 5 C**, the O_2^- signals of CoS_x QDs 1:0.5 and 1:2 samples were stronger than 1:4 samples after reaction for 5 and 10 min, while no significant difference was detected within the initial 2 min. This phenomenon indicated that CoS_x QDs 1:0.5 and 1:2 samples exhibited more persistent O_2^- generation abilities compared with CoS_x QDs 1:4, which resulted from their higher defects degree that provide more active sites for radical generation. More importantly, the O_2^- signals of CoS_x QDs 1:2 were higher than 1:0.5 sample, which might be attributed that the existence of Co^{3+} in CoS_x QDs 1:2 accelerated defect consumption and generated more radical in a certain time. Similar phenomenon could also be found from DMPO-•OH signal, except that the •OH signal of CoS_x QDs 1:0.5 at first 2 min was higher than other two samples (**Figure S7**). Combined with the above-mentioned characterization and analyses, this phenomenon might be related to valence of cobalt and sulfur vacancy density in defect-engineered CoS_x QDs. The mechanism of defect engineered

CoS_x QDs for photothermal-enhanced Fenton-like reaction could be described as follows and shown in Equation (1)-(3): hydroxyl radicals (•OH) is generated from H_2O_2 by the oxidation of Co^{2+} [Eqs. (1)]. Then, Co^{3+} reduced to Co^{2+} by H_2O_2, accompanied by the production of O_2 and $2H^+$ [Eqs. (2)]. Simultaneously, the bound O_2 could be reduced to O_2^- by the sulfur defect [Eqs. (3)]. CoS_x QDs 1:0.5 showed the most persistent process of ROS generation, which could be attributed to an abundant sulfur vacancy defect. Even so, its reaction at first 10 min was still lower than that of CoS_x QDs 1:2, proving that the intrinsic co-existence of Co^{2+}/Co^{3+} could accelerate ROS generation in the early stage of the reaction. As sulfur amount increased, the extent of Fenton-like reaction diminished due to limited sulfur defect.

$$H_2O_2 + Co^{2+} \rightarrow Co^{3+} + \bullet OH + OH^- \quad (1)$$

$$H_2O_2 + Co^{3+} \rightarrow Co^{2+} + O_2 + 2H^+ \quad (2)$$

$$O_2 + e^- (\text{defect}) \rightarrow O_2^- \quad (3)$$

In conclusion, the valence state ratio of Co^{2+}/Co^{3+} and sulfur defect level could co-regulate the catalytic rate of Fenton-like reaction and total ROS production, confirming the possibility of tunable PTT-enhanced CDT by defect engineering of CoS_x QDs.

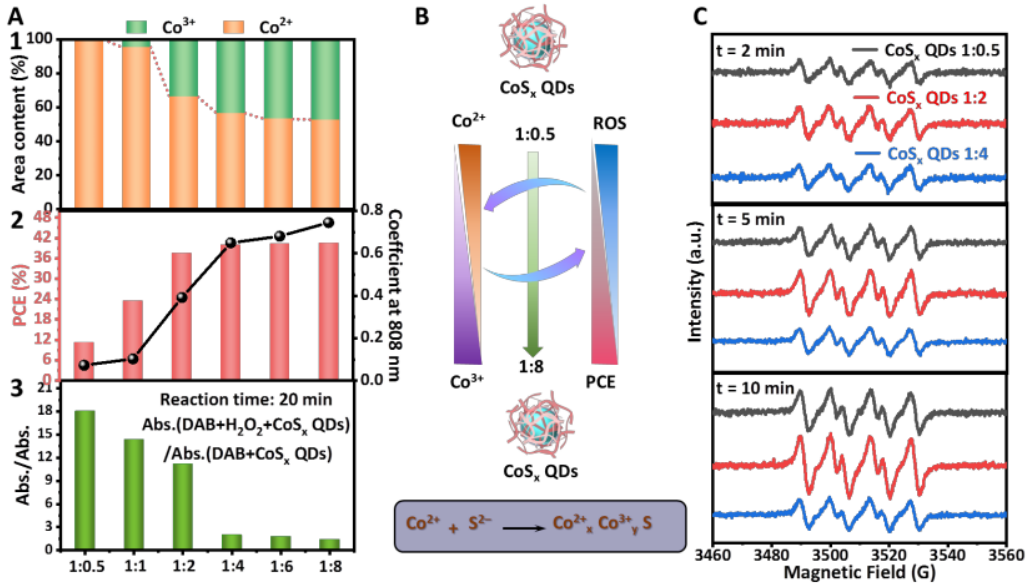

Figure 5. Defect-dependent photothermal effect and Fenton-like activity of CoS_x QDs. (**A**) The influence of valence state changes of cobalt in photothermal effect and Fenton-like reaction, (**A1**) the area content of Co^{2+} and Co^{3+} obtained from Co 2p XPS spectra, (**A2**) the PCEs and molar absorption coefficient at 808 nm, (**A3**) the comparison of catalytic effect after 20 min; (**B**) Schematic illustration for mechanism of photothermal amplified chemodynamic effect; (**C**) ESR spin trap signals of DMPO-O_2^- under different conditions.

Biocompatibility of the CoS_x QDs and their high specificity of cytotoxicity on cancer cells. Inspired by the results of above extracellular experiments, the CoS_x QDs are expected to induce cancer cell apoptosis by the synergy effect of PTT, CDT and GSH depletion. The possible schematic mechanism was displayed in **Figure 6A**. Considering that the weakly-acidic tumor microenvironment can enhance the •OH production capacity and promote the self-disintegration of CoS_x QDs, this in turn further exposes more surface defects for higher Fenton-like reaction rate. We then investigated the synergistic CDT/PTT effect in cancer cell lines. Firstly, the biocompatibility of un-irradiated CoS_x QDs was confirmed on LO2, A431, MDA-MB-231 and 4T1 cells with standard MTT experiments (**Figure 6B**). The viability of LO2, A431, MDA-MB-231 cells were greater than 95 % after incubating with non-irradiated CoS_x QDs 1:2 for 24 h even at a high concentration up to 1.0 mM, which confirmed the low toxicity of CoS_x QDs. However, the cell viabilities of 4T1 cells were dose-dependent and decreased to 60 % at the concentration of 1 mM CoS_x QDs. The different survival rates may be attributed to the higher basal level of oxidative stress in 4T1 cells than cancer A431 cells,[43] MDA-MB-231 cells[44,45] and normal LO2 cells, that in turn produced more •OH via Fenton-like reactions even when there was no laser irradiation. Therefore, the CDT capability of the CoS_x QDs was dependent on the oxidative state of the cells. Then the synergetic anticancer effect of CDT and PTT was investigated by treating 4T1 and A431 cells with CoS_x QDs 1:2 and exposure to 808 nm NIR laser for 5 min, as depicted in **Figure 6C-D**. This is due to that a slightly acidic pH 6.5 environments could accelerate Fenton-like reaction of CoS_x QDs to produce more •OH, inducing the significantly decreased cell viability of 4T1cells, further indicating the high CDT efficiency of CoS_x QDs in tumor microenvironment. Notably, without laser irradiation, cell viability of A431 cells

remained relatively high even up to 1mM concentration of CoS_x QDs. However, under laser irradiation at 808 nm for 5 min, the cell viability of both 4T1 and A431 decreased significantly when CoS_x QDs were irradiated with the 808 nm laser, confirming the synergistic killing effect of PTT alone and PTT-enhanced CDT.

Moreover, *in vitro* PTT and PTT-enhanced CDT efficacy of CoS_x QDs was further visually confirmed by confocal fluorescence imaging of 4T1 cells and A431 incubated with CoS_x QDs 1:2, live-dead stained with calcein AM and propidium iodide (PI), respectively (**Figure 6E**, **F**). It can be clearly observed that the red spots in 4T1cells both greatly increased with CoS_x QDs concentrations with and without laser irradiation, while that in CoS_x QDs treated A431 cells only enhanced with laser irradiation. Notably, both two cells without CoS_x QDs treatment were not affected even after laser irradiation at the power density of 0.8 W/cm^2 for 5 min. This means that CoS_x QDs have higher capability to ablate 4T1 cells than A431cells no matter with and without laser irradiation, which is consistence with the result of Figure 6B. Such phenomena may be attributed to higher H_2O_2 generation in CoS_x QDs treated 4T1 cells than other three cell lines.[43-45] Moreover, imaging quantification showed that the ratios of average ratios of the red fluorescence intensity to green fluorescence intensity from CoS_x QDs treated and untreated cells (**Figure 6G**, **H**). The ratios for 4T1 cells decreased significantly with increasing CoS_x QDs 1:2 concentrations with and without laser irradiation, wherein they sustainably suffered a greater fall without than with laser irradiation at the same concentrations of CoS_x QDs. By contrast, this high killing effect trend was repeatedly observed with A431 cells but only for the laser irradiation group. These data verified that CoS_x QDs were promising candidates for anticancer therapeutics due to the synergetic effect of CDT and PTT.

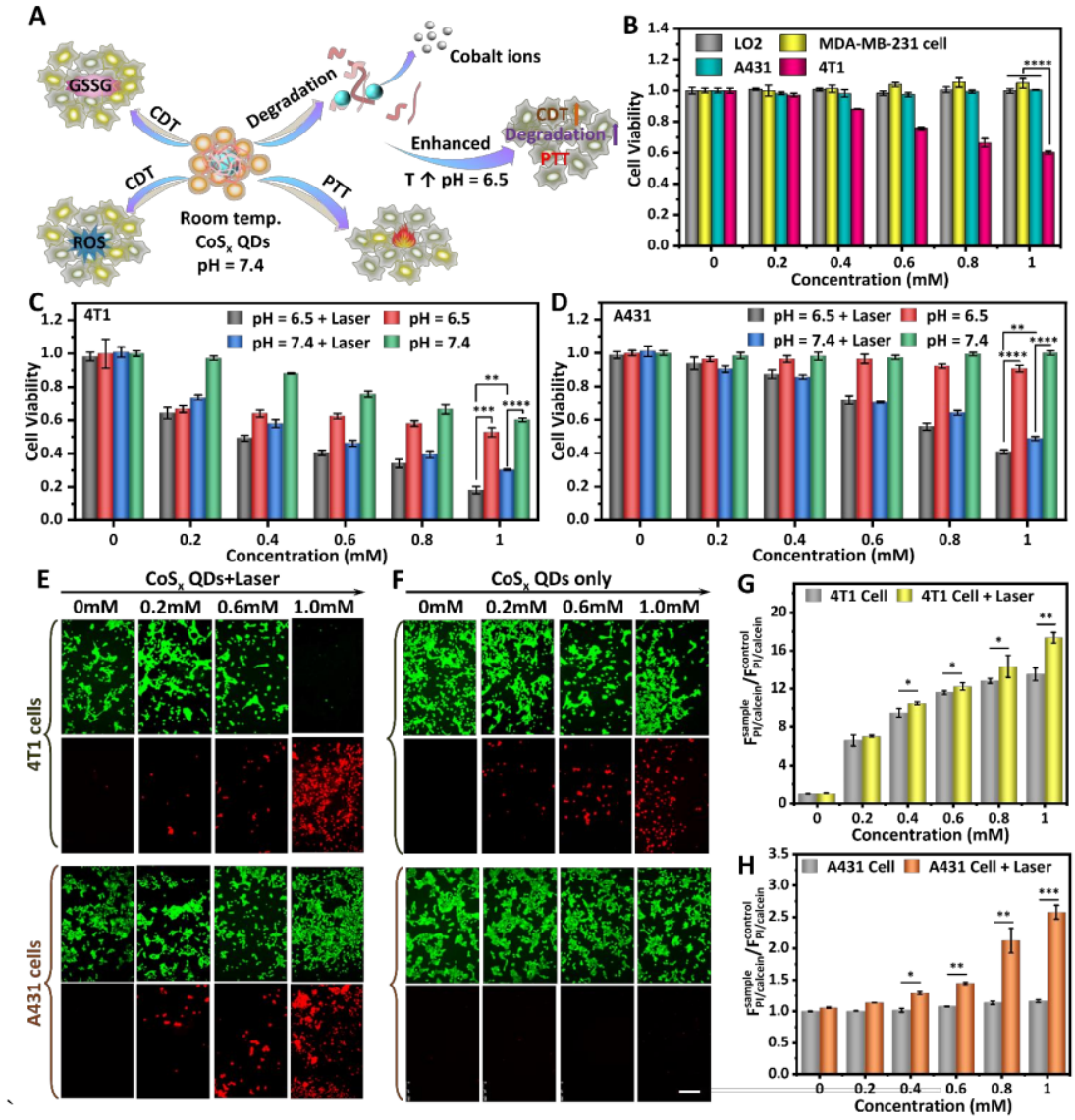

Figure 6. ***In vitro*** **PTT and hyperthermal-enhanced CDT of cancer cells by biodegradable CoS_x QDs.** (**A**) Schematic mechanism for biodegradable CoS_x QDs induced cancer cell apoptosis; (**B**) Relative viabilities of four cell lines incubated with CoS_x QDs 1:2 at different concentrations for 24 h; (**C-D**) Cell viability of A431 and 4T1 cells treated with various concentrations of CoS_x QDs 1:2 at pH 7.4 and 6.5 under 808 nm laser irradiation (power density: 0.8 W/cm^2). Fluorescence images of A431 and 4T1cells with (**E**) or without laser irradiation (**F**) stained with calcein AM/PI under different conditions. Scale bar: 200 μm. Quantification of dead and live 4T1 (**G**) and A431 (**H**) cells stained with calcein AM/PI with and without laser treatment. The data show mean ± s.d., n = 8 (**B**), n = 5 (**C**, **D**, **G** and **H**). *P < 0.05, **P <

0.01, ***P < 0.001, and ****P < 0.0001, analyzed by Student's t-test (**B, G** and **H**) or two-way ANOVA (**C** and **D**) with Tukey's multiple comparisons post-test. Asterisks indicate statistically significant differences between CoS_x QDs + laser groups *vs* CoS_x QDs only groups.

Synergistic photothermal and chemodynamic therapy of CoS_x QDs *in vivo*. Encouraged by the promising photothermal and Fenton-like performance in *in vitro* cell culture models, the *in vivo* antitumor therapeutic efficacy of the CoS_x QDs was further evaluated. The 4T1 tumor-bearing nude mice were randomly divided into four groups, including control group (saline), saline + laser group (saline plus 808 nm laser irradiation), CoS_x QDs group and CoS_x QDs + laser group (CoS_x QDs plus 808 nm laser irradiation). In laser irradiation groups, the tumor sites were irradiated by 808 nm laser (0.8 W/cm^2) at 6 h post-injection. After 8 min of laser irradiation, the tumor temperature of mice in saline injection group did not have obvious changes, while the temperature of tumor areas of mice in CoS_x QDs injection group rapidly increased and reached the plateau of ~ 52 °C (**Figure 7A** and **7B**). These results indicated the good *in vivo* photothermal effect of CoS_x QDs, which was sufficient to induce hyperthermia for tumor inhibition. The tumor volume of each group was measured and recorded with time (**Figure 7C**). Each tumor was collected and weighed after different treatments for 22 days (**Figure 7D** and **7E**). For saline + laser group, the tumor grew rapidly with an insignificant inhibition rate of ~ 4 %. Compared to the rapid tumor growth in the control group, the tumor growth in CoS_x QDs group was significantly inhibited, which should be ascribed to the high •OH generation ability of CoS_x QDs in tumor microenvironment. However, the tumor inhibition ratio in CoS_x QDs group was ~ 39.5 %, indicating that Fenton-like reaction of the CoS_x QDs alone could not achieve desired therapeutic effect. Distinct from above three groups, the tumor growth in CoS_x QDs + laser group was completely inhibited, revealing the improved therapeutic effect of CDT in combination with PTT.

Malignant tumors are prone to metastasis, thereby forming distant tumors, which is the main cause of tumor death. Therefore, the inhibition effect of CoS_x QDs in distant tumors was also investigated. As shown in the lung tissue photograph (**Figure 7F**), obvious metastatic tumor nodules were observed in the lungs in saline group, saline + laser group and CoS_x QDs group, whereas which could not be observed in

the lungs for CoS_x QDs + laser group, suggesting remarkable synergistic therapy effect of PTT and PTT-enhanced CDT killing of the primary tumor such that there was not sufficient surviving cancer cells to undergo metastasis.

Furthermore, the fascinating therapeutic effect *in vivo* was also evaluated by collecting tumor tissues after various treatments for H&E, Ki67 antigen and terminal deoxynucleotidyl transferase (TUNEL) staining, respectively. As displayed in **Figure 7G**, the most serious tumor cell damage such as condensed nucleus, more vacuoles and changed cellular morphology was found in mice treated with CoS_x QDs + laser group, which further show the high synergism of PTT with PTT-enhanced CDT killing efficiency *in vivo*. The body weights of mice in all groups increased slowly with time and showed no noticeable difference during the therapeutic process (**Figure 7H**). Their major organs were collected for histology analysis after H&E staining (**Figure 7I**). No obvious histological damage was observed on organ slices for all groups, which demonstrated favorable biocompatibility of CoS_x QDs.

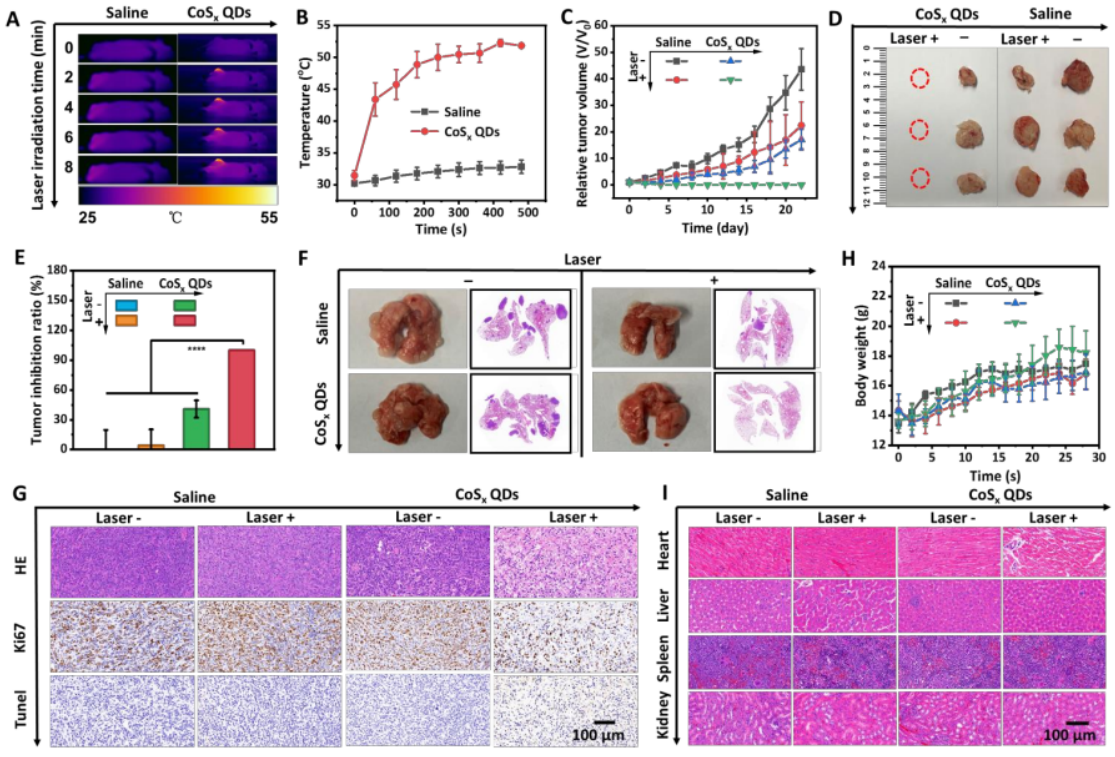

Figure 7. ***In vivo*** **synergistic PTT and hyperthermal-enhanced CDT of CoS_x QDs.** (**A**) Infrared thermal images of 4T1 tumor-bearing mice under laser irradiation at 808 nm (0.8 W/cm^2) for 8 min after intravenous injection of saline or CoS_x QDs 1:2 and (**B**) corresponding temperature variation curves of tumor sites; (**C**) Tumor growth curves of different groups of mice after injection of saline or CoS_x QDs 1:2 with and without laser irradiation; (**D**) Digital photographs of excised tumors and (**E**) the tumor inhibition rate received various treatments for 22 days. The data are presented as the mean ± s.d., n = 3. The statistical significance was calculated via two-way ANOVA with Tukey's multiple comparisons test. ****$p < 0.0001$. (**F**) Digital photographs and H&E staining images of lungs in mice after different treatments; (**G**) H&E, Ki67 antigen and TUNEL staining images of tumor tissues harvested from corresponding mice after 15 days of various treatments; (**H**) Body weight data. (**I**) H&E staining images of main organs (heart, liver, spleen and kidney) in different groups. Different treatment conditions included saline and 3.75 μg/mL of CoS_x QDs 1:2.

CONCLUSION

In summary, we have developed a facile and novel strategy to obtain biodegradable CoS_x QDs in a mild condition and employ it for the synergistic PTT and hyperthermal CDT. Defect engineering of CoS_x QDs was induced to regulate its PTT and CDT performance by the tunable sulfur vacancy density on the surface. The experimental results confirmed the as-prepared CoS_x QDs 1:2 exhibited excellent Fenton-like property and photothermal performance simultaneously, and its therapeutic effect was enhanced by both the rise of local temperature of tumor and higher catalytic rate of Fenton-like reaction under laser irradiation. Meanwhile, the partial and gradual biodegradability of CoS_x QDs into cobalt ions would not only improve the ROS generation ability by increasing crystal defect density but also possibly facilitated eventual elimination of CoS_x QDs from the body after their therapeutic outcomes were achieved. The XRD and XPS results confirmed the PCEs increased with the increasing of trivalent cobalt (Co^{3+}), while the chemodynamic effect decreased with the increasing of Co^{3+}, which indicated the synergistic effect of PTT/CDT could be regulated by controlling the intrinsic valance state of cobalt in CoS_x QDs. The cell experiments proved the biocompatibility of CoS_x QDs for normal cells. By photothermal-enhanced Fenton-like reaction, CoS_x QDs could produce sufficient ROS for cell inactivation without extrinsic addition of H_2O_2.

METHODS

Materials. All chemicals and reagents (analytical grade) were used as received without any further purification. Cobalt chloride ($CoCl_2•6H_2O$), sodium sulfide ($Na_2S•9H_2O$), bovine serum album (BSA) and 3,3′-diaminobenzidine tetrahydrochloride tablet (DAB) were purchased from Sigma-Aldrich Co. (USA). The 3,3′-diaminobenzidine tetrahydrochloride tablet contains two kinds of tablets (DAB and H_2O_2), dissolve them in 5 mL water to obtain storage solution, respectively. 3,3',5,5'-tetramethylbenzidine dihydrochloride (TMB) and methylene blue (MB) were purchased from Marklin Chemical Co., Ltd (China). Ultrapure water was obtained from a Milli-Q system (Health Force Biomeditech Holdings Ltd.).

Material Characterization. TEM images were obtained on a JEM 1400 transmission electron microscope with an accelerating voltage from 40 to 120 kV. UV-vis absorption spectra were determined by PerkinElmer UV-vis spectrophotometer. DLS was performed on the Malvern Nano-ZS Particle Size. IR thermal image was recorded by the photothermal camera FLIR T420. The contents of cobalt ions in those samples were determined by using inductively coupled plasma atomic-emission spectroscopy (ICP-AES, Thermo). The binding energy of the sample were characterized by X-ray photoelectron spectroscopy (XPS; AXIS HIS, Kratos Analytical). The powder XRD measurements were performed using a Bruker D8 advanced diffractometer with a Cu Ka irradiation in the 2θ range of 200-600. Dynamic light scattering (DLS) measurements were performed at room temperature with a Zetasizer Nano ZS (Malvern Instruments). The recorded intensity autocorrelation function was transformed into number functions to investigate particle size distribution. ESR spectra were obtained using a Bruker A300-10/12 ESR spectrometer (center field: 3480.00 G; microwave frequency: 9.79 GHz; and power: 5.05 mW) to trap the active oxygen species (•HO, O_2^-, etc.). An 808 nm high power NIR Laser (operating mode, CW; output power after fiber, 2.5 W; LED dis- play, diode current, multimode fiber; fiber core diameter, 400 μm; fiber connector, SMA905, with tunable laser driver module of 0%–100%) purchased from CNI Co., Ltd. was used for PTT experiments. The laser spot size was 1 cm^2. It was used as the surface laser and position on top of the mice. The laser power was measured by laser power meter.

Synthesis of CoS_x QDs. In a typical procedure, the Co-precursor solution was firstly prepared by dispersing 0.5 mL Co^{2+} solution (0.1 M) and 40 mg BSA into 40 mL water, and the pH value was adjusted into 3.0 by 1 M HCl. Then, 0.2 mL Na_2S (0.5 M) was dropped slowly under vigorous stirring at room temperature. After adjusting pH value to neutral, a clear black solution of CoS_x QDs 1:2 was produced quickly. Then the obtained black solution was purified by ultrafiltration centrifuge tube (MWCO 5000) and centrifuged in 4°C for several times. The concentration of CoS_x QDs was measured by ICP. Also, CoS_x QDs with other defect level were prepared by adding different volumes of Na_2S solution.

Quantitative Measurement of Photothermal Conversion Efficiency of CoS_x QDs. The solution temperatures were monitored by using an IR thermal camera. Experiments were taken out in 0.2 mL 1 × PBS solutions (pH = 6.5) containing different concentrations of CoS_x QDs. When the samples were exposed to laser of 808 nm (0.8 W/cm^2), the temperature was recorded every 20 s for 5 min, then turned off the laser and recorded the temperature declining process of the samples. To explore the photothermal conversion stability of the CoS_x QDs, its aqueous dispersion (Co ion concentration of 1 mM) was irradiated by the NIR-laser (0.8 W/cm^2) for 5 min, then the laser was off for 5 min to cool the sample. The on/off irradiation cycle was repeated for five times.

The photothermal conversion efficiency (PCE) was calculated according to the previous literature.

$$\eta = \frac{hS(T_{max} - T_{sur}) - Q_{dis}}{I(1 - 10^{-A_{808}})}$$

η is the photothermal conversion efficiency, T_{max} is the equilibrium temperature for solution, T_{sur} is the surrounding temperature. Q_{dis} is the heat loss. I is the incident laser power, and A is the absorbance of CoS_x QDs solution at 808 nm.

$$\tau_s = \frac{m_D C_D}{hS}$$

m_D is the mass of solvent (0.2 g) and C_D is the heat capacity [4.2 ×10^3 J/ (kg °C)]. τ_s is the sample system time constant.

Fenton-Like Reaction of CoS_x QDs. In this part, DAB, TMB and MB were used to assess the amount of ROS generated by the Fenton-like reaction. For the DAB oxidation, 50 μL CoS_x QDs (2 mM), 200 μL DAB solution and 200 μL H_2O_2 solution were mixed in 550 μL 1 × PBS solutions (pH = 6.5) at 20 °C. After the addition of CoS_x QDs, the UV–vis–NIR absorbance of the mixed system at a range of 200-800 nm was measured. To assess the influence of defect level on the •OH production rate, UV kinetics was investigated at 569 nm. For the TMB oxidation, 50 μL CoS_x QDs (2 mM) were mixed with 0.6 mM TMB in 1 × PBS solutions (pH = 6.5) and incubated with H_2O_2 (10 mM). The UV kinetics of TMB oxidation system was investigated at 665 nm. For the degradation of MB, 25 mM $NaHCO_3$/5% CO_2 buffer solution containing 5 mg/L MB, 10 mM H_2O_2, and 0.2 mM CoS_x QDs was allowed to stand at room temperature for 30 min. The UV kinetics of MB degradation system was investigated at 665 nm. All reactions were taken out at room temperature (~ 20 °C).

***In Vitro* Thermal Enhanced Fenton-Like Reaction.** The *in vitro* experiments were taken out in digital heating circulating water bath, which can provide a stable reaction temperature that easy to avoid the accumulation of errors during heating process. First, 200 μL DAB, 200 μL H_2O_2 and 550 μL 1 × PBS solutions (pH = 6.5) were mixed in quartz cuvette and was heated in a water bath for 10 minutes. After the pretreatment, 50 μL CoS_x QDs 1:2 was added into the solution and then recorded the absorbance by UV spectrum every minute to monitor the extent of reaction. In this part, three different temperatures (20, 40 and 50 °C) were taken to test the effect of temperature on CDT efficacy.

Cytotoxicity Assay and Cellular Uptake of CoS_x QDs. The *in vitro* cytotoxicity was measured using Alamar Blue viability assay. Four cell lines including human hepatic cell (LO2), human epidermoid carcinoma cell (A431), human epithelial breast cell (MDA-MB-231) and mouse breast cancer cell (4T1) were cultured in Dulbecco's Modified Eagle Medium (DMEM) containing 10 % fetal bovine serum in a humidified environment containing 5 % CO_2 and 95 % air at 37 °C. 4T1 cells were seeded in 96-well plates (Costar, IL, U.S.A.) at an intensity of 3×10^4 cells/mL. After 24 h incubation, the medium was replaced by fresh medium containing CoS_x QDs 1:2 suspensions at different concentrations, and the cells

were then incubated for 24. After the designated time intervals, the Alamar Blue reagent was added into cell culture medium in 1 to 10 volume ratios for cell incubation. 3 h later in an incubator, fluorescent measurement (Ex.: 560 nm, Em.: 590 nm) was taken and normalized against untreated samples to the cell viability.

***In Vitro* Photothermal Ablation of CoS_x QDs.** A431 cells and 4T1 cells were cultured in Lab-Tek chambered cover-glass (ThermoFisher) with the growth medium (DMEM supplemented with 10 % fetal bovine serum and 1 % penicillin–streptomycin; ThermoFisher), at 37 °C in a humidified atmosphere containing 5 % CO_2 and 95 % air. After incubation for 24 h, A431 cells and 4T1 cells were firstly exposed to various concentrations of CoS_x QDs 1:2 and irradiated by an 808 nm laser (0.8 W/cm^2) for 5 min at pH 6.5 and pH 7.4, respectively. These cells were incubated for an additional 24 h, and relative cell viabilities were determined by the standard Alamar Blue assay mentioned above. For further studying *in vitro* PTT effect, cells seeded into 8 well plates were incubated with 0.2, 0.6 and 1.0 mM of CoS_x QDs 1:2 and then irradiated by an 808-nm laser (0.8 W/cm^2) for 5 min. The cells were stained with Calcein AM and Propidium Iodide (PI) for 30 min, washed with PBS, and then imaged by a confocal fluorescence microscope (Leica, SP8).

Statistical Analysis. Data was expressed as mean ± SD. The statistical significance of the data was compared by Student's t-test. Analysis of variance (ANOVA) was used to analyze the differences among the different groups.

Establishment of Tumor Models. To prepare the tumor model, 1.0 × 10^6 4T1 cells were suspended in PBS (50 μL) and subcutaneously injected into the right back region of four-week-old nude mice. When the tumor diameter reached about 8–10 mm, the tumor-bearing mice were used for *in vivo* therapy.

***In Vivo* Photothermal Studies.** To evaluate the photothermal property in vivo, the 4T1 tumor-bearing nude mice were injected with saline or CoS_x QDs *via* the tail vein, the dosage of the injected nanoparticles was at an equivalent dose of CPT at 3 mg/kg. The laser irradiation (808 nm, 0.8 W/cm^2, 8

min) was performed at 6 h after injection. The temperature of tumor regions was detected using an infrared thermography camera (E40, FLIR) at the desired the irradiation time point.

***In Vivo* Synergistic PTT/CDT.** The tumor-bearing nude mice were divided into four groups randomly (n = 3, in each group), and injected via tail vein with saline only, injected with saline plus laser (808 nm, 0.8 W/cm^2, 8 min), CoS_x QDs dispersion only (5 mg mL^{-1}, 50 μL), and CoS_x QDs plus laser (808 nm, 0.8 W/cm^2, 8 min), respectively. During the irradiation, the temperature of mice body was monitored by an IR thermal imager. After the treatment, tumor size and body weight of each mouse were measured every two days. And the tumor growth inhibition rate (TGIR) was calculated according to the equation: TGIR(%) = (1 – G/G0) × 100% The tissues of major organs of the mice were stained by hematoxylin and eosin (H&E) and imaged using an inverted fluorescence microscope (IX71, Olympus, Japan) for histology analysis. All animal experiments were carried out under protocols approved by the Institutional Animal Care and Use Committee. The approval number of animals is IACUC-2019021.

ASSOCIATED CONTENT

Supporting Information. Supplementary figures S1-S2: in vitro characterization of nanoparticles including DLS and XRD analysis, bandgap energy measurements of CoS_x QDs solution, additional figures S4-S7 presented the measurement of ROS generation using different methods including UV−vis spectra and corresponding dynamics analysis of Fenton-like reaction process and ESR spin trap signals under different conditions. These supplementary informations are available online.

AUTHOR INFORMATION

Corresponding Author

David Tai Leong- Department of Chemical and Biomolecular Engineering, Faculty of Engineering, National University of Singapore, Singapore 117585, Singapore. Email: cheltwd@nus.edu.sg

Suhua Wang-College of Environmental Science and Engineering, North China Electric Power University, Beijing 102206, P. R. China. Guangdong Provincial Key Laboratory of Petrochemical Pollution Process and Control, School of Environmental Science and Engineering, Guangdong University of Petrochemical Technology, Maoming, Guangdong 525000, P. R. China. Email: wangsh@gdupt.edu.cn

Houjuan Zhu-Department of Chemical and Biomolecular Engineering, Faculty of Engineering, National University of Singapore, Singapore 117585, Singapore. Institute of Materials Research and Engineering, A*STAR (Agency for Science, Technology and Research), Singapore 138634, Singapore. Email: zhu_houjuan@imre.a-star.edu.sg

Jingchao Li-Shanghai Engineering Research Center of Nano-Biomaterials and Regenerative Medicine, College of Chemistry, Chemical Engineering and Biotechnology, Donghua University, Shanghai 201620, P.R. China. Email:jcli@dhu.edu.cn

Author

Shuyi Huang-College of Environmental Science and Engineering, North China Electric Power University, Beijing 102206, P. R. China Department of Chemical and Biomolecular Engineering, National University of Singapore, 4 Engineering Drive 4, Singapore 117585, Singapore

Mengbin Ding-Shanghai Engineering Research Center of Nano-Biomaterials and Regenerative Medicine, College of Chemistry, Chemical Engineering and Biotechnology, Donghua University, Shanghai 201620, P.R. China

Zibiao Li-Institute of Materials Research and Engineering, A*Star (Agency for Science, Technology and Research), Singapore, Singapore

ACKNOWLEDGEMENTS

This work was supported by the National Natural Science Foundation of China (82001957, 21775042 and 22176044), the National Key Research and Development Program of China (2017YFA0207003), Projects

of Talents Recruitment of GDUPT (2019rc056, and 2019rc057) and National University of Singapore Reimagine Grant (R279000627114).

REFERENCE

[1]. Chang, M.; Wang, M.; Shu, M.; Ding, B.; Li, C.; Pang, M.; Cui, S.; Hou, Z.; Lin, J., A Multifunctional Cascade Bioreactor Based on Hollow-Structured Cu_2MoS_4 for Synergetic Cancer Chemo-Dynamic Therapy/Starvation Therapy/Phototherapy/Immunotherapy with Remarkably Enhanced Efficacy. *Adv Mater* **2019,** *31* (51), e1905271.

[2]. Lin, H.; Chen, Y.; Shi, J., Nanoparticle-triggered in situ catalytic chemical reactions for tumour-specific therapy. *Chem Soc Rev* **2018,** *47* (6), 1938-1958.

[3]. Tang, Z.; Zhang, H.; Liu, Y.; Ni, D.; Zhang, J.; Yao, Z.; He, M.; Shi, J.; Bu, W., Antiferromagnetic Pyrite as the Tumor Microenvironment-Mediated Nanoplatform for Self-Enhanced Tumor Imaging and Therapy. *Adv Mater* **2017,** *29* (47).

[4]. Wu, W.; Yu, L.; Jiang, Q.; Huo, M.; Lin, H.; Wang, L.; Chen, Y.; Shi, J., Enhanced Tumor-Specific Disulfiram Chemotherapy by In Situ Cu(2+) Chelation-Initiated Nontoxicity-to-Toxicity Transition. *J Am Chem Soc* **2019,** *141* (29), 11531-11539.

[5]. Zhu, H.; Fang, Y.; Miao, Q.; Qi, X.; Ding, D.; Chen, P.; Pu, K., Regulating Near-Infrared Photodynamic Properties of Semiconducting Polymer Nanotheranostics for Optimized Cancer Therapy. *ACS Nano* **2017,** *11* (9), 8998-9009.

[6]. Zhu, H.; Lai, Z.; Fang, Y.; Zhen, X.; Tan, C.; Qi, X.; Ding, D.; Chen, P.; Zhang, H.; Pu, K., Ternary Chalcogenide Nanosheets with Ultrahigh Photothermal Conversion Efficiency for Photoacoustic Theranostics. *Small* **2017,** *13* (16).

[7]. Zhu, H.; Li, J.; Qi, X.; Chen, P.; Pu, K., Oxygenic Hybrid Semiconducting Nanoparticles for Enhanced Photodynamic Therapy. *Nano Lett* **2018,** *18* (1), 586-594.

[8]. Hu, Y.; Lv, T.; Ma, Y.; Xu, J.; Zhang, Y.; Hou, Y.; Huang, Z.; Ding, Y., Nanoscale Coordination Polymers for Synergistic NO and Chemodynamic Therapy of Liver Cancer. *Nano Lett* **2019,** *19* (4), 2731-2738.

[9]. Lei, S.; Chen, J.; Zeng, K.; Wang, M.; Ge, X., Visual Dual Chemodynamic/Photothermal Therapeutic Nanoplatform Based on Superoxide Dismutase plus Prussian Blue. *Nano Res* **2019,** *12* (5), 1071–1082.

[10]. Zhang, C.; Yan, L.; Wang, X.; Dong, X.; Zhou, R.; Gu, Z.; Zhao, Y., Tumor Microenvironment-Responsive $Cu_2(OH)PO_4$ Nanocrystals for Selective and Controllable Radiosentization via the X-ray-Triggered Fenton-like Reaction. *Nano Lett* **2019,** *19* (3), 1749-1757.

[11]. Sang, Y.; Cao, F.; Li, W.; Zhang, L.; You, Y.; Deng, Q.; Dong, K.; Ren, J.; Qu, X., Bioinspired Construction of a Nanozyme-Based H_2O_2 Homeostasis Disruptor for Intensive Chemodynamic Therapy. *J Am Chem Soc* **2020,** *142* (11), 5177-5183.

[12]. Ma, B.; Wang, S.; Liu, F.; Zhang, S.; Duan, J.; Li, Z.; Kong, Y.; Sang, Y.; Liu, H.; Bu, W.; Li, L., Self-Assembled Copper-Amino Acid Nanoparticles for in Situ Glutathione "AND" H_2O_2 Sequentially Triggered Chemodynamic Therapy. *J Am Chem Soc* **2019,** *141* (2), 849-857.

[13]. Liu, Y.; Jia, Q.; Guo, Q.; Wei, W.; Zhou, J., Simultaneously activating highly selective ratiometric MRI and synergistic therapy in response to intratumoral oxidability and acidity. *Biomaterials* **2018,** *180*, 104-116.

[14]. Wang, X.; Zhong, X.; Zha, Z.; He, G.; Miao, Z.; Lei, H.; Luo, Q.; Zhang, R.; Liu, Z.; Cheng, L., Biodegradable CoS_2 Nanoclusters for Photothermal-Enhanced Chemodynamic Therapy. *Appl Mater Today* **2020,** *18*, 100464.

[15]. He, S.; Jiang, Y.; Li, J.; Pu, K., Semiconducting Polycomplex Nanoparticles for Photothermal Ferrotherapy of Cancer. *Angew Chem Int Ed Engl* **2020,** *59* (26), 10633-10638.

[16]. Liu, Y.; Zhen, W.; Wang, Y.; Liu, J.; Jin, L.; Zhang, T.; Zhang, S.; Zhao, Y.; Song, S.; Li, C.; Zhu, J.; Yang, Y.; Zhang, H., One-Dimensional Fe_2P Acts as a Fenton Agent in Response to NIR II Light and Ultrasound for Deep Tumor Synergetic Theranostics. *Angew Chem Int Ed Engl* **2019,** *58* (8), 2407-2412.

[17]. Jiang, C.; He, T.; Tang, Q.; He, J.; Ren, Q.; Zhang, D.-Y.; Gurram, B.; Blum, N. T.; Chen, Y.; Huang, P., Nanozyme Catalyzed Cascade Reaction for Enhanced Chemodynamic Therapy of Low-H_2O_2 Tumor. *Appl Mater Today* **2022,** *26*, 101357.

[18]. Zhen, X.; Xie, C.; Pu, K., Temperature-Correlated Afterglow of a Semiconducting Polymer Nanococktail for Imaging-Guided Photothermal Therapy. *Angew Chem Int Ed Engl* **2018,** *57* (15), 3938-3942.

[19]. Liu, F.; Lin, L.; Zhang, Y.; Wang, Y.; Sheng, S.; Xu, C.; Tian, H.; Chen, X., A Tumor-Microenvironment-Activated Nanozyme-Mediated Theranostic Nanoreactor for Imaging-Guided Combined Tumor Therapy. *Adv Mater* **2019,** *31* (40), e1902885.

[20]. Zhu, H.; Li, Z.; Ye, E.; Leong, D. T., Oxygenic Enrichment in Hybrid Ruthenium Sulfide Nanoclusters for an Optimized Photothermal Effect. *ACS Appl Mater Interfaces* **2021,** *13* (50), 60351-60361.

[21]. He, T.; Yuan, Y.; Jiang, C.; Blum, N. T.; He, J.; Huang, P.; Lin, J., Light-Triggered Transformable Ferrous Ion Delivery System for Photothermal Primed Chemodynamic Therapy. *Angew Chem Int Ed Engl* **2021,** *60* (11), 6047-6054.

[22]. Chen, Y.; Li, Z. H.; Pan, P.; Hu, J. J.; Cheng, S. X.; Zhang, X. Z., Tumor-Microenvironment-Triggered Ion Exchange of a Metal-Organic Framework Hybrid for Multimodal Imaging and Synergistic Therapy of Tumors. *Adv Mater* **2020,** *32* (24), e2001452.

[23]. Cheng, W.; Nie, J.; Gao, N.; Liu, G.; Tao, W.; Xiao, X.; Jiang, L.; Liu, Z.; Zeng, X.; Mei, L., A Multifunctional Nanoplatform against Multidrug Resistant Cancer: Merging the Best of Targeted Chemo/Gene/Photothermal Therapy. *Adv Funct Mater* **2017,** *27* (45), 1704135.

[24]. Chen, S.; Lei, Q.; Qiu, W. X.; Liu, L. H.; Zheng, D. W.; Fan, J. X.; Rong, L.; Sun, Y. X.; Zhang, X. Z., Mitochondria-targeting "Nanoheater" for enhanced photothermal/chemo-therapy. *Biomaterials* **2017,** *147*, 92-104.

[25]. Eftekhari, A., Tungsten Dichalcogenides (WS_2, WSe_2, and WTe_2): Materials Chemistry and Applications. *J Mater Chem A Mater* **2017,** *5* (35), 18299–18325.

[26]. Ji, J.; Yan, Q.; Yin, P.; Mine, S.; Matsuoka, M.; Xing, M., Defects on CoS_{2-x} : Tuning Redox Reactions for Sustainable Degradation of Organic Pollutants. *Angew Chem Int Ed Engl* **2021,** *60* (6), 2903-2908.

[27]. Tian, J.; Zhu, H.; Chen, J.; Zheng, X.; Duan, H.; Pu, K.; Chen, P., Cobalt Phosphide Double-Shelled Nanocages: Broadband Light-Harvesting Nanostructures for Efficient Photothermal Therapy and Self-Powered Photoelectrochemical Biosensing. *Small* **2017,** *13* (22).

[28]. He, T.; Jiang, C.; He, J.; Zhang, Y.; He, G.; Wu, J.; Lin, J.; Zhou, X.; Huang, P., Manganese-Dioxide-Coating-Instructed Plasmonic Modulation of Gold Nanorods for Activatable Duplex-Imaging-Guided NIR-II Photothermal-Chemodynamic Therapy. *Adv Mater* **2021,** *33* (13), e2008540.

[29]. Ding, X.; Peng, F.; Zhou, J.; Gong, W.; Slaven, G.; Loh, K. P.; Lim, C. T.; Leong, D. T., Defect engineered bioactive transition metals dichalcogenides quantum dots. *Nat Commun* **2019,** *10* (1), 41.

[30]. Wang, Z.; Huang, P.; Jacobson, O.; Liu, Y.; Lin, L.; Lin, J.; Lu, N.; Zhang, H.; Tian, R.; Niu, G.; Liu, G.; Chen, X., Biomineralization-Inspired Synthesis of Copper Sulfide-Ferritin Nanocages as Cancer Theranostics. *ACS Nano* **2016,** *10* (3), 3453-60.

[31]. Dong, Z.; Feng, L.; Hao, Y.; Chen, M.; Gao, M.; Chao, Y.; Zhao, H.; Zhu, W.; Liu, J.; Liang, C.; Zhang, Q.; Liu, Z., Synthesis of Hollow Biomineralized $CaCO_3$-Polydopamine Nanoparticles for Multimodal Imaging-Guided Cancer Photodynamic Therapy with Reduced Skin Photosensitivity. *J Am Chem Soc* **2018,** *140* (6), 2165-2178.

[32]. Yang, C.; Younis, M. R.; Zhang, J.; Qu, J.; Lin, J.; Huang, P., Programmable NIR-II Photothermal-Enhanced Starvation-Primed Chemodynamic Therapy using Glucose Oxidase-Functionalized Ancient Pigment Nanosheets. *Small* **2020,** *16* (25), e2001518.

[33]. Dhenadhayalan, N.; Lin, T.-W.; Lee, H.-L.; Lin, K.-C., Multisensing Capability of MoSe2 Quantum Dots by Tuning Surface Functional Groups. *ACS Appl Nano Mater* **2018,** *1* (7), 3453–3463.

[34]. Kim, M. J.; Jeon, S. J.; Kang, T. W.; Ju, J. M.; Yim, D.; Kim, H. I.; Park, J. H.; Kim, J. H., 2H-WS2 Quantum Dots Produced by Modulating the Dimension and Phase of 1T-Nanosheets for Antibody-Free Optical Sensing of Neurotransmitters. *ACS Appl Mater Interfaces* **2017,** *9* (14), 12316-12323.

[35]. Zhu, H.; Ni, N.; Govindarajan, S.; Ding, X.; Leong, D. T., Phototherapy with layered materials derived quantum dots. *Nanoscale* **2020,** *12* (1), 43-57.

[36]. Vines, J. B.; Yoon, J. H.; Ryu, N. E.; Lim, D. J.; Park, H., Gold Nanoparticles for Photothermal Cancer Therapy. *Front Chem* **2019,** *7*, 167.

[37]. Xu, J. W.; Yao, K.; Xu, Z. K., Nanomaterials with a photothermal effect for antibacterial activities: an overview. *Nanoscale* **2019,** *11* (18), 8680-8691.

[38]. Fernandes, N.; Rodrigues, C. F.; Moreira, A. F.; Correia, I. J., Overview of the application of inorganic nanomaterials in cancer photothermal therapy. *Biomater Sci* **2020,** *8* (11), 2990-3020.

[39]. Zheng, M.; Yue, C.; Ma, Y.; Gong, P.; Zhao, P.; Zheng, C.; Sheng, Z.; Zhang, P.; Wang, Z.; Cai, L., Single-step assembly of DOX/ICG loaded lipid--polymer nanoparticles for highly effective chemo-photothermal combination therapy. *ACS Nano* **2013,** *7* (3), 2056-67.

[40]. Ju, E.; Dong, K.; Chen, Z.; Liu, Z.; Liu, C.; Huang, Y.; Wang, Z.; Pu, F.; Ren, J.; Qu, X., Copper(II)-Graphitic Carbon Nitride Triggered Synergy: Improved ROS Generation and Reduced Glutathione Levels for Enhanced Photodynamic Therapy. *Angew Chem Int Ed Engl* **2016,** *55* (38), 11467-71.

[41]. Zhang, C.; Bu, W.; Ni, D.; Zhang, S.; Li, Q.; Yao, Z.; Zhang, J.; Yao, H.; Wang, Z.; Shi, J., Synthesis of Iron Nanometallic Glasses and Their Application in Cancer Therapy by a Localized Fenton Reaction. *Angew Chem Int Ed Engl* **2016,** *55* (6), 2101-6.

[42]. Fu, L. H.; Qi, C.; Hu, Y. R.; Lin, J.; Huang, P., Glucose Oxidase-Instructed Multimodal Synergistic Cancer Therapy. *Adv Mater* **2019,** *31* (21), e1808325.

[43]. He, T.; Qin, X.; Jiang, C.; Jiang, D.; Lei, S.; Lin, J.; Zhu, W. G.; Qu, J.; Huang, P., Tumor pH-responsive metastable-phase manganese sulfide nanotheranostics for traceable hydrogen sulfide gas therapy primed chemodynamic therapy. *Theranostics* **2020,** *10* (6), 2453-2462.

[44]. Pandey, R. R.; Guo, Y.; Gao, Y.; Chusuei, C. C., A Prussian Blue ZnO Carbon Nanotube Composite for Chronoamperometrically Assaying H2O2 in BT20 and 4T1 Breast Cancer Cells. *Anal Chem* **2019,** *91* (16), 10573-10581.

[45]. Dong, W.; Ren, Y.; Bai, Z.; Yang, Y.; Chen, Q., Fabrication of hexahedral Au-Pd/graphene nanocomposites biosensor and its application in cancer cell H_2O_2 detection. *Bioelectrochemistry* **2019,** *128*, 274-282.

Table of Contents

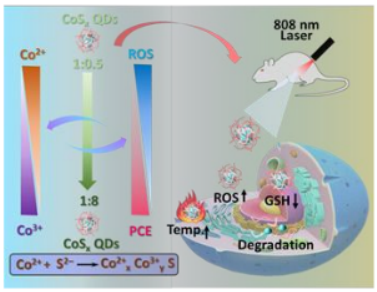

Sulfur Defect Engineered Biodegradable Cobalt Sulfide Quantum Dots Driven Photothermal and Chemodynamic Anti-Cancer Therapy

ORIGINALITY REPORT

39%
SIMILARITY INDEX

PRIMARY SOURCES

1	Houjuan Zhu, Zibiao Li, Enyi Ye, David Tai Leong. "Oxygenic Enrichment in Hybrid Ruthenium Sulfide Nanoclusters for an Optimized Photothermal Effect", ACS Applied Materials & Interfaces, 2021 Crossref	328 words — 3%
2	Yuanlin Wang, Zhenglin Li, Ying Hu, Jing Liu et al. "Photothermal conversion-coordinated Fenton-like and photocatalytic reactions of Cu2-xSe-Au Janus nanoparticles for tri-combination antitumor therapy", Biomaterials, 2020 Crossref	264 words — 2%
3	jnanobiotechnology.biomedcentral.com Internet	252 words — 2%
4	www.mdpi.com Internet	209 words — 2%
5	Houjuan Zhu, Zhuangchai Lai, Yuan Fang, Xu Zhen, Chaoliang Tan, Xiaoying Qi, Dan Ding, Peng Chen, Hua Zhang, Kanyi Pu. "Ternary Chalcogenide Nanosheets with Ultrahigh Photothermal Conversion Efficiency for Photoacoustic Theranostics", Small, 2017 Crossref	203 words — 2%
6	dr.ntu.edu.sg	

Internet

179 words — 2%

7 Houjuan Zhu, Yuan Fang, Qingqing Miao, Xiaoying Qi, Dan Ding, Peng Chen, Kanyi Pu. "Regulating Near-Infrared Photodynamic Properties of Semiconducting Polymer Nanotheranostics for Optimized Cancer Therapy", ACS Nano, 2017
Crossref

157 words — 1%

8 pubs.rsc.org
Internet

118 words — 1%

9 wjgnet.com
Internet

115 words — 1%

10 pubs.acs.org
Internet

92 words — 1%

11 Jie Wang, Lijia Yao, Enlai Hu, Yuanjing Cui, Deren Yang, Guodong Qian. "MnO2 decorated ZIF-8@GOx for synergistic chemodynamic and starvation therapy of cancer", Journal of Solid State Chemistry, 2021
Crossref

85 words — 1%

12 Fan Jiang, Binbin Ding, Shuang Liang, Yajie Zhao, Ziyong Cheng, Bengang Xing, Ping'an Ma, Jun Lin. "Intelligent MoS2–CuO heterostructures with multiplexed imaging and remarkably enhanced antitumor efficacy via synergetic photothermal therapy/ chemodynamic therapy/ immunotherapy", Biomaterials, 2021
Crossref

84 words — 1%

13 Yanhong Sun, Hongda Chen, Ying Huang, Fengqin Xu, Guifeng Liu, Lina Ma, Zhenxin Wang. "One-pot synthesis of AuPd@FexOy Nanoagent with the activable Fe

75 words — 1%

species for Enhanced Chemodynamic-Photothermal Synergetic Therapy", Biomaterials, 2021
Crossref

14 ouci.dntb.gov.ua
Internet
75 words — 1%

15 Lu Lu, Kui Wang, Chuanchuan Lin, Weihu Yang, Qiaojian Duan, Ke Li, Kaiyong Cai. "Constructing nanocomplexes by multicomponent self-assembly for curing orthotopic glioblastoma with synergistic chemo-photothermal therapy", Biomaterials, 2021
Crossref
69 words — 1%

16 www.nature.com
Internet
65 words — 1%

17 Jun Zhao, Shuyi Huang, Priyaharshini Ravisankar, Houjuan Zhu. "Two-Dimensional Nanomaterials for Photoinduced Antibacterial Applications", ACS Applied Bio Materials, 2020
Crossref
59 words — 1%

18 Shuyi Huang, Long Yu, Pengchen Su, Tao Wen, Mingtai Sun, Dejian Huang, Xiangke Wang, Suhua Wang. "Surface enhanced FRET for sensitive and selective detection of doxycycline using organosilicon nanodots as donors", Analytica Chimica Acta, 2022
Crossref
56 words — 1%

19 www.dovepress.com
Internet
55 words — 1%

20 www.researchgate.net
Internet
55 words — 1%

21 Penghui Cheng, Kanyi Pu. "Activatable Phototheranostic Materials for Imaging-Guided Cancer Therapy", ACS Applied Materials & Interfaces, 2019
Crossref
51 words — < 1%

22 Xiao Liu, Yilan Jin, Tingting Liu, Shengju Yang, Mengxue Zhou, Weiqi Wang, Haijun Yu. "Iron-Based Theranostic Nanoplatform for Improving Chemodynamic Therapy of Cancer", ACS Biomaterials Science & Engineering, 2020
Crossref
47 words — < 1%

23 pubmed.ncbi.nlm.nih.gov
Internet
46 words — < 1%

24 Chunyan Guo, Jinghua Sun, Jie Dong, Wenwen Cai, Xuhui Zhao, Bin Song, Ruiping Zhang. "Natural Anthocyanin-Based Multifunctional Theranostic Agent for Dual-Modal Imaging and Photothermal Anti-Tumor Therapy", Journal of Materials Chemistry B, 2021
Crossref
43 words — < 1%

25 Yite Li, Junli Zhou, Lei Wang, Zhigang Xie. "Endogenous Hydrogen Sulfide-Triggered MOF-based Nanoenzyme for Synergic Cancer Therapy", ACS Applied Materials & Interfaces, 2020
Crossref
43 words — < 1%

26 ddd.uab.cat
Internet
43 words — < 1%

27 Shuaitian Guo, Ran Li, Fangzhen Tian, Xueting Yang, Li Wang, Shanyue Guan, Shuyun Zhou, Jun Lu. "Carbon-Defect-Driven Boron Carbide for Dual-Modal NIR-II/Photoacoustic Imaging and Photothermal Therapy", ACS Biomaterials Science & Engineering, 2021
Crossref
42 words — < 1%

28	link.springer.com Internet	42 words — < 1%
29	Pengcheng Gu, Sai Zhang, Ran Ma, Mingtai Sun, Suhua Wang, Tao Wen, Xiangke Wang. "Layered double hydroxides nanosheets in-situ anchored on ultrathin MXenes for enhanced U(VI) and Eu(III) trapping: Excavating from selectivity to mechanism", Separation and Purification Technology, 2022 Crossref	41 words — < 1%
30	Yayu Wen, Xu Chen, Xufeng Zhu, Youcong Gong, Guanglong Yuan, Xiuying Qin, Jie Liu. "Photothermal-Chemotherapy Integrated Nanoparticles with Tumor Microenvironment Response Enhanced the Induction of Immunogenic Cell Death for Colorectal Cancer Efficient Treatment", ACS Applied Materials & Interfaces, 2019 Crossref	41 words — < 1%
31	Yite Li, Junli Zhou, Lei Wang, Zhigang Xie. "Endogenous Hydrogen Sulfide-Triggered MOF-Based Nanoenzyme for Synergic Cancer Therapy", ACS Applied Materials & Interfaces, 2020 Crossref	41 words — < 1%
32	www.thno.org Internet	39 words — < 1%
33	www.ccmu.edu.cn Internet	36 words — < 1%
34	Xianwen Wang, Xiaoyan Zhong, Zhengbao Zha, Gang He, Zhaohua Miao, Huali Lei, Qunyi Luo, Rui Zhang, Zhuang Liu, Liang Cheng. "Biodegradable CoS2 nanoclusters for photothermal-enhanced chemodynamic therapy", Applied Materials Today, 2020 Crossref	34 words — < 1%

35	Houjuan Zhu, Jingchao Li, Xiaoying Qi, Peng Chen, Kanyi Pu. "Oxygenic Hybrid Semiconducting Nanoparticles for Enhanced Photodynamic Therapy", Nano Letters, 2017 Crossref	33 words — < 1%
36	thno.org Internet	33 words — < 1%
37	uwspace.uwaterloo.ca Internet	33 words — < 1%
38	Yangju Li, Haoran Dong, Long Li, Junyang Xiao, Shuangjie Xiao, Zilan Jin. "Efficient degradation of sulfamethazine via activation of percarbonate by chalcopyrite", Water Research, 2021 Crossref	30 words — < 1%
39	Chanchan Yu, Lanju Xu, Yuanyuan Zhang, Peter S. Timashev, Yuanyu Huang, Xing-Jie Liang. "Polymer-Based Nanomaterials for Noninvasive Cancer Photothermal Therapy", ACS Applied Polymer Materials, 2020 Crossref	29 words — < 1%
40	Jiansheng Liu, Xueqin Qing, Qin Zhang, Ningyue Yu, Mengbin Ding, Zhaohui Li, Zhen Zhao, Zhiling Zhou, Jingchao Li. "Oxygen-producing proenzyme hydrogels for photodynamic mediated metastasis-inhibited combinational therapy", Journal of Materials Chemistry B, 2021 Crossref	29 words — < 1%
41	Ranhao Yin, Hongwei Ge, Hui Chen, Jingjing Du, Zhenli Sun, Hua Tan, Suhua Wang. "Sensitive and rapid detection of trace microplastics concentrated through Au-nanoparticle-decorated sponge on the basis of surface-	29 words — < 1%

enhanced Raman spectroscopy", Environmental Advances, 2021
Crossref

42 Xin Liu, Yang Liu, Yijun Guo, Wei Shi, Yanan Sun, Zi He, Yuqing Shen, Xiuming Zhang, Haihua Xiao, Dongtao Ge. "Metabolizable pH/H2O2 dual-responsive conductive polymer nanoparticles for safe and precise chemo-photothermal therapy", Biomaterials, 2021 — 29 words — < 1%
Crossref

43 www.acsu.buffalo.edu — 29 words — < 1%
Internet

44 Huihui Wang, Lili Zhang, Chun Hu, Xiangke Wang, Lai Lyu, Guodong Sheng. "Enhanced degradation of organic pollutants over Cu-doped LaAlO 3 perovskite through heterogeneous Fenton-like reactions", Chemical Engineering Journal, 2018 — 28 words — < 1%
Crossref

45 Pradipta Behera, Ashutosh Mohanty, Mrinmoy De. "Functionalized Fluorescent Nanodots for Discrimination of Nitroaromatic Compounds", ACS Applied Nano Materials, 2020 — 28 words — < 1%
Crossref

46 Yanjuan Sang, Fangfang Cao, Wei Li, Lu Zhang, Yawen You, Qingqing Deng, Kai Dong, Jinsong Ren, Xiaogang Qu. " Bioinspired Construction of a Nanozyme-Based H O Homeostasis Disruptor for Intensive Chemodynamic Therapy ", Journal of the American Chemical Society, 2020 — 25 words — < 1%
Crossref

47 cpb-us-e2.wpmucdn.com — 25 words — < 1%
Internet

48	opac.wsb.torun.pl Internet	25 words — < 1%
49	Mukaddes Izci, Christy Maksoudian, Bella B. Manshian, Stefaan J. Soenen. "The Use of Alternative Strategies for Enhanced Nanoparticle Delivery to Solid Tumors", Chemical Reviews, 2021 Crossref	24 words — < 1%
50	tel.archives-ouvertes.fr Internet	24 words — < 1%
51	par.nsf.gov Internet	21 words — < 1%
52	www.rsc.org Internet	19 words — < 1%
53	Savchuk, Ol.A., J.J. Carvajal, J. Massons, M. Aguiló, and F. Díaz. "Determination of photothermal conversion efficiency of graphene and graphene oxide through an integrating sphere method", Carbon, 2016. Crossref	18 words — < 1%
54	Zheng Deng, Chao Fang, Xu Ma, Xiang Li, Yu-Jia Zeng, Xinsheng Peng. "One Stone Two Birds: Zr-Fc Metal–Organic Framework Nanosheet for Synergistic Photothermal and Chemodynamic Cancer Therapy", ACS Applied Materials & Interfaces, 2020 Crossref	16 words — < 1%
55	Zhenghuan Zhao, Kai Xu, Chen Fu, Heng Liu, Ming Lei, Jianfeng Bao, Ailing Fu, Yang Yu, Weiguo Zhang. "Interfacial engineered gadolinium oxide nanoparticles for magnetic resonance imaging guided microenvironment-	16 words — < 1%

mediated synergetic chemodynamic/photothermal therapy", Biomaterials, 2019
Crossref

56 riubu.ubu.es
Internet
16 words — < 1%

57 Dejun She, Shaojun Peng, Li Liu, Huihui Huang, Yingyan Zheng, Yiping Lu, Daoying Geng, Bo Yin. "Biomimic FeS2 nanodrug with hypothermal photothermal effect by clinical approved NIR- II light for augmented chemodynamic therapy", Chemical Engineering Journal, 2020
Crossref
15 words — < 1%

58 Jiayong Dai, Jibin Song, Yuan Qiu, Jingjing Wei, Zhongzhu Hong, Lei Li, Huanghao Yang. " Gold Nanoparticle-Decorated g-C N Nanosheets for Controlled Generation of Reactive Oxygen Species upon 670 nm Laser Illumination ", ACS Applied Materials & Interfaces, 2019
Crossref
15 words — < 1%

59 Sainan Liu, Ying Zhou, Chunling Hu, Lihan Cai, Maolin Pang. "Covalent Organic Framework-Based Nanocomposite for Synergetic Photo-, Chemodynamic-, and Immunotherapies", ACS Applied Materials & Interfaces, 2020
Crossref
15 words — < 1%

60 Wensheng Xie, Zhenhu Guo, Qin Gao, Dan Wang, Kang Liang, Zi Gu, Lingyun Zhao. "Manganese-Doped Layered Double Hydroxide: A Biodegradable Theranostic Nanoplatform with Tumor Microenvironment Response for Magnetic Resonance Imaging-Guided Photothermal Therapy", ACS Applied Bio Materials, 2020
Crossref
15 words — < 1%

61 www.pnas.org
Internet

15 words — < 1%

62 Bin Liu, Yulong Bian, Shuang Liang, Meng Yuan, Shuming Dong, Fei He, Shili Gai, Piaoping Yang, Ziyong Cheng, Jun Lin. "One-Step Integration of Tumor Microenvironment-Responsive Calcium and Copper Peroxides Nanocomposite for Enhanced Chemodynamic/Ion-Interference Therapy", ACS Nano, 2021
Crossref
14 words — < 1%

63 Bin Liu, Zhao Wang, Tianyao Li, Qianqian Sun, Shuming Dong, Chongna Zhong, Dan Yang, Fei He, Shili Gai, Piaoping Yang. "Rapid Decomposition and Catalytic Cascade Nanoplatforms Based on Enzymes and Mn-Etched Dendritic Mesoporous Silicon for MRI-Guided Synergistic Therapy", ACS Applied Materials & Interfaces, 2020
Crossref
14 words — < 1%

64 Tao Bao, Wenyan Yin, Xiaopeng Zheng, Xiao Zhang et al. "One-pot synthesis of PEGylated plasmonic MoO3–x hollow nanospheres for photoacoustic imaging guided chemo-photothermal combinational therapy of cancer", Biomaterials, 2016
Crossref
13 words — < 1%

65 Tingting Xiao, Meijuan He, Fang Xu, Yu Fan, Bingyang Jia, Mingwu Shen, Han Wang, Xiangyang Shi. "Macrophage Membrane-Camouflaged Responsive Polymer Nanogels Enable Magnetic Resonance Imaging-Guided Chemotherapy/Chemodynamic Therapy of Orthotopic Glioma", ACS Nano, 2021
Crossref
13 words — < 1%

66 worldwidescience.org
Internet
12 words — < 1%

67 Bing Guo, Zonghai Sheng, Dehong Hu, Anran Li et al. "Molecular Engineering of Conjugated Polymers for Biocompatible Organic Nanoparticles with Highly Efficient Photoacoustic and Photothermal Performance in Cancer Theranostics", ACS Nano, 2017
Crossref
11 words — < 1%

68 doaj.org
Internet
11 words — < 1%

69 Caina Xu, Yanbing Wang, Haiyang Yu, Huayu Tian, Xuesi Chen. "Multifunctional Theranostic Nanoparticles Derived from Fruit-Extracted Anthocyanins with Dynamic Disassembly and Elimination Abilities", ACS Nano, 2018
Crossref
10 words — < 1%

70 Hui Peng, Ya-Ting Qin, Yu-Sheng Feng, Xi-Wen He, Wen-You Li, Yu-Kui Zhang. "Phosphate-Degradable Nanoparticles Based on Metal–Organic Frameworks for Chemo-Starvation-Chemodynamic Synergistic Antitumor Therapy", ACS Applied Materials & Interfaces, 2021
Crossref
10 words — < 1%

71 Jiahui Ji, Qingyun Yan, Pengcheng Yin, Shinya Mine, Masaya Matsuoka, Mingyang Xing. " Defects on CoS : Tuning Redox Reactions for Sustainable Degradation of Organic Pollutants ", Angewandte Chemie, 2020
Crossref
10 words — < 1%

72 Wei Zhang, Wenhai Lin, Xin Wang, Chaonan Li, Shi Liu, Zhigang Xie. "Hybrid Nanomaterials of Conjugated Polymers and Albumin for Precise Photothermal Therapy", ACS Applied Materials & Interfaces, 2018
Crossref
10 words — < 1%

73 Wei Zhou, Haidi Guan, Kaiyao Sun, Yuxin Xing, Jixi Zhang. "FeOOH/Polypyrrole Nanocomposites with an Islands-in-Sea Structure toward Combined Photothermal/Chemodynamic Therapy", ACS Applied Bio Materials, 2019
Crossref
10 words — < 1%

74 Yan Lyu, Yuan Fang, Qingqing Miao, Xu Zhen, Dan Ding, Kanyi Pu. " Intraparticle Molecular Orbital Engineering of Semiconducting Polymer Nanoparticles as Amplified Theranostics for Photoacoustic Imaging and Photothermal Therapy ", ACS Nano, 2016
Crossref
10 words — < 1%

75 Zhao Wang, Bin Liu, Qianqian Sun, Shuming Dong, Ye Kuang, Yushan Dong, Fei He, Shili Gai, Piaoping Yang. "Fusiform-Like Copper(II)-Based Metal–Organic Framework through Relief Hypoxia and GSH-Depletion Co-Enhanced Starvation and Chemodynamic Synergetic Cancer Therapy", ACS Applied Materials & Interfaces, 2020
Crossref
10 words — < 1%

76 thesesups.ups-tlse.fr
Internet
10 words — < 1%

77 www.chinchemlett.com.cn
Internet
10 words — < 1%

78 Kexin Bian, Xuwu Zhang, Kai Liu, Tian Yin, Huan Liu, Kang Niu, Weiwei Cao, Dawei Gao. "Peptide-Directed Hierarchical Mineralized Silver Nanocages for Anti-Tumor Photothermal Therapy", ACS Sustainable Chemistry & Engineering, 2018
Crossref
9 words — < 1%

79 Li Yang, Xiao-Jiao Zhu, Min Qu, Tian-Ren Xu, Ya-Min Ye, Zi-Zhen Zeng, Jie Zhang, Lian-ke Wang, Zhi-Peng
9 words — < 1%

Yu, Hong-Ping Zhou. "In-Situ-Bloomed Micrometer-Scale Ultrathin Nanosheets in Tumor-Microenvironment for Intensive Photothermal-Enhanced Chemodynamic Therapy", ACS Applied Bio Materials, 2021
Crossref

80 Lian-Hua Fu, Yan-Ru Hu, Chao Qi, Ting He, Shanshan Jiang, Chao Jiang, Jin He, Junle Qu, Jing Lin, Peng Huang. "Biodegradable Manganese-Doped Calcium Phosphate Nanotheranostics for Traceable Cascade Reaction-Enhanced Anti-Tumor Therapy", ACS Nano, 2019 — 9 words — < 1%
Crossref

81 Qing Chen, Su He, Fangjun Zhang, Fengzhi Cui, Jianhua Liu, Man Wang, Dongmei Wang, Zhigang Jin, Chunxia Li. "多功能Pt-Ce6纳米平台作为过氧化氢纳米酶和NIR-II光热剂用于增强PDT/PTT肿瘤治疗", Science China Materials, 2020 — 9 words — < 1%
Crossref

82 Www.dovepress.com — 9 words — < 1%
Internet

83 Yong Qian, Jiahui Zhang, Jinglu Zou, Xingyu Wang et al. "NIR-II responsive PEGylated nickel nanoclusters for photothermal enhanced chemodynamic synergistic oncotherapy", Theranostics, 2022 — 9 words — < 1%
Crossref

84 Aftab Nadeem, Alexandra Berg, Hudson Pace, Athar Alam et al. " Protein-lipid interaction at low pH induces oligomerisation of the MakA cytotoxin from ", Cold Spring Harbor Laboratory, 2021 — 8 words — < 1%
Crossref Posted Content

85 Bo Zhou, Bang-Ping Jiang, Wanying Sun, Fang-Mian Wei, Yun He, Hong Liang, Xing-Can Shen. "Water- — 8 words — < 1%

Dispersible Prussian Blue Hyaluronic Acid Nanocubes with Near-Infrared Photoinduced Singlet Oxygen Production and Photothermal Activities for Cancer Theranostics", ACS Applied Materials & Interfaces, 2018
Crossref

86 Chen Dai, Shengjian Zhang, Zhuang Liu, Rong Wu, Yu Chen. "Two-Dimensional Graphene Augments Nanosonosensitized Sonocatalytic Tumor Eradication", ACS Nano, 2017 — 8 words — < 1%
Crossref

87 Kefyalew Dagnew Addisu, Balkew Zewge Hailemeskel, Shewaye Lakew Mekuria, Abegaz Tizazu Andrgie, Yu-Chun Lin, Hsieh-Chih Tsai. "Bioinspired, Manganese-Chelated Alginate-Poly(Dopamine) Nanomaterials for Efficient In Vivo T1-Weighted Magnetic Resonance Imaging (MRI)", ACS Applied Materials & Interfaces, 2017 — 8 words — < 1%
Crossref

88 Meng He, Chang Du, Jindong Xia, Zhi-Gang Zhang, Chang-Ming Dong. "Multivalent Polypeptide and Tannic Acid Cooperatively Iron-Coordinated Nanohybrids for Synergistic Cancer Photothermal Ferroptosis Therapy", Biomacromolecules, 2022 — 8 words — < 1%
Crossref

89 Qi Wang, Dongguang Niu, Jinsheng Shi, Lili Wang. "A Three-in-one ZIFs-Derived CuCo(O)/GOx@PCNs Hybrid Cascade Nanozyme for Immunotherapy/Enhanced Starvation/Photothermal Therapy", ACS Applied Materials & Interfaces, 2021 — 8 words — < 1%
Crossref

90 Weitao Yang, Xiudong Shi, Yuxin Shi, Defan Yao, Shizhen Chen, Xin Zhou, Bingbo Zhang. "Beyond the Roles in Biomimetic Chemistry: An Insight into the Intrinsic — 8 words — < 1%

Catalytic Activity of an Enzyme for Tumor-Selective Phototheranostics", ACS Nano, 2018
Crossref

91 Xiangqi Liu, Wei Feng, Huijing Xiang, Baihui Liu, Mujie Ye, Meng Wei, Rui Dong, Yu Chen, Kuiran Dong. "Multifunctional Cascade Nanocatalysts for NIR-II-Synergized Photonic Hyperthermia-Strengthened Nanocatalytic Therapy of Epithelial and Embryonal Tumors", Chemical Engineering Journal, 2021 — 8 words — < 1%
Crossref

92 Yang Liu, Wenyao Zhen, Yinghui Wang, Shuyan Song, Hongjie Zhang. " Na S O Nanoparticles Trigger Antitumor Immunotherapy through Reactive Oxygen Species Storm and Surge of Tumor Osmolarity ", Journal of the American Chemical Society, 2020 — 8 words — < 1%
Crossref

93 Yang Liu, Ying Wang, Wenyao Zhen, Yinghui Wang, Songtao Zhang, Ying Zhao, Shuyan Song, Zhijian Wu, Hongjie Zhang. "Defect modified zinc oxide with augmenting sonodynamic reactive oxygen species generation", Biomaterials, 2020 — 8 words — < 1%
Crossref

94 Yanyan Cui, Jian Yang, Qunfang Zhou, Ping Liang, Yaling Wang, Xueyun Gao, Yongtian Wang. "Renal Clearable Ag Nanodots for in Vivo Computer Tomography Imaging and Photothermal Therapy", ACS Applied Materials & Interfaces, 2017 — 8 words — < 1%
Crossref

95 Yingnan Liu, Zhirong Guo, Fan Li, Yaqing Xiao, Yalan Zhang, Tong Bu, Pei Jia, Taotao Zhe, Li Wang. "Multifunctional Magnetic Copper Ferrite Nanoparticles as Fenton-like Reaction and Near-Infrared Photothermal Agents — 8 words — < 1%

for Synergetic Antibacterial Therapy", ACS Applied Materials & Interfaces, 2019
Crossref

96	oar.a-star.edu.sg Internet	8 words — < 1%
97	uknowledge.uky.edu Internet	8 words — < 1%
98	www.gmp-chitosan.com Internet	8 words — < 1%
99	www.mei.nus.edu.sg Internet	8 words — < 1%
100	Haili Yan, Long Gao, You Liao, Dongmei Wang, Duiping Feng, Jianguo Li, Jiangfeng Du, Zhanjun Gu, Hui Zhang. "Hexagonal NaxWO3 Nanocrystals with Reversible Valence States for Microwave thermal and Chemodynamic Combined Cancer Therapy", Chemical Engineering Journal, 2022 Crossref	7 words — < 1%
101	Sun, Xiaolian, Xinglu Huang, Xuefeng Yan et al. "Chelator-Free 64Cu-Integrated Gold Nanomaterials for Positron Emission Tomography Imaging Guided Photothermal Cancer Therapy", ACS Nano Crossref	7 words — < 1%
102	Wencheng Wu, Luodan Yu, Quzi Jiang, Minfeng Huo, Han Lin, Liying Wang, Yu Chen, Jianlin Shi. " Enhanced Tumor-Specific Disulfiram Chemotherapy by Cu Chelation-Initiated Nontoxicity-to-Toxicity Transition ", Journal of the American Chemical Society, 2019 Crossref	7 words — < 1%

103 Ye Zhang, Yi Cao, Tian Gao, Ye Kuang, Zhen An, Zheng Mao, Yilin He, Jincong Yan, Zhongzhong Lu, Renjun Pei. "A Tumor Microenvironment-Responsive and Catalytic Cascade-Enhanced Nanocomposite for Tumor Thermal Ablation Synergizing with Chemodynamic and Chemotherapy", ACS Applied Bio Materials, 2020
Crossref
7 words — < 1%

104 hdl.handle.net
Internet
7 words — < 1%

105 Dalong Ni, Carolina A. Ferreira, Todd E. Barnhart, Virginia Quach et al. "Magnetic Targeting of Nanotheranostics Enhances Cerenkov Radiation-Induced Photodynamic Therapy", Journal of the American Chemical Society, 2018
Crossref
6 words — < 1%

106 Kuan Hu, Lin Xie, Yiding Zhang, Masayuki Hanyu et al. "Marriage of black phosphorus and Cu2+ as effective photothermal agents for PET-guided combination cancer therapy", Nature Communications, 2020
Crossref
6 words — < 1%

107 Xianwen Wang, Xiaoyan Zhong, Huali Lei, Yuehao Geng, Qi Zhao, Fei Gong, Zhijuan Yang, Ziliang Dong, Zhuang Liu, Liang Cheng. " Hollow Cu Se Nanozymes for Tumor Photothermal-Catalytic Therapy ", Chemistry of Materials, 2019
Crossref
6 words — < 1%

108 Youjuan Wang, Linan Shi, Zhifei Ye, Kesong Guan, Lili Teng, Jianghong Wu, Xia Yin, Guosheng Song, Xiao-Bing Zhang. "Reactive Oxygen Correlated Chemiluminescent Imaging of a Semiconducting Polymer
6 words — < 1%

Nanoplatform for Monitoring Chemodynamic Therapy", Nano Letters, 2019
Crossref

109 Zi He, Huiling Su, Yuqing Shen, Wei Shi, Xin Liu, Yang Liu, Fuhui Zhang, Yansheng Zhang, Yanan Sun, Dongtao Ge. "Poly(norepinephrine)-coated FeOOH nanoparticles as carriers of artemisinin for cancer photothermal-chemical combination therapy", RSC Advances, 2019 — 6 words — < 1%
Crossref

110 Ziliang Dong, Hua Gong, Min Gao, Wenwen Zhu, Xiaoqi Sun, Liangzhu Feng, Tingting Fu, Yonggang Li, Zhuang Liu. "Polydopamine Nanoparticles as a Versatile Molecular Loading Platform to Enable Imaging-guided Cancer Combination Therapy", Theranostics, 2016 — 6 words — < 1%
Crossref

EXCLUDE QUOTES	OFF	EXCLUDE SOURCES	OFF
EXCLUDE BIBLIOGRAPHY	OFF	EXCLUDE MATCHES	OFF